Field- and pressure-induced magnetic quantum phase transitions in $TlCuCl_3$

Masashige Matsumoto,[1,2] B. Normand,[3] T. M. Rice,[1] and Manfred Sigrist[1]
[1]*Theoretische Physik, ETH-Hönggerberg, CH-8093 Zürich, Switzerland*
[2]*Department of Physics, Faculty of Science, Shizuoka University, 836 Oya, Shizuoka 422-8529, Japan*
[3]*Département de Physique, Université de Fribourg, CH-1700 Fribourg, Switzerland*
(Received 15 September 2003; published 25 February 2004)

Thallium copper chloride is a quantum spin liquid of $S=1/2$ Cu^{2+} dimers. Interdimer superexchange interactions give a three-dimensional magnon dispersion and a spin gap significantly smaller than the dimer coupling. This gap is closed by an applied hydrostatic pressure of approximately 2 kbar or by a magnetic field of 5.6 T, offering a unique opportunity to explore both types of quantum phase transition and their associated critical phenomena. We use a bond-operator formulation to obtain a continuous description of all disordered and ordered phases, and thus of the transitions separating these. Both pressure- and field-induced transitions may be considered as the Bose–Einstein condensation of triplet magnon excitations, and the respective phases of staggered magnetic order as linear combinations of dimer-singlet and dimer-triplet modes. We focus on the evolution with applied pressure and field of the magnetic excitations in each phase, and in particular on the gapless (Goldstone) modes in the ordered regimes which correspond to phase fluctuations of the ordered moment. The bond-operator description yields a good account of the magnetization curves and of magnon dispersion relations observed by inelastic neutron scattering under applied fields, and a variety of experimental predictions for pressure-dependent measurements.

DOI: 10.1103/PhysRevB.69.054423 PACS number(s): 75.10.Jm, 75.40.Cx, 75.40.Gb

I. INTRODUCTION

Thallium copper chloride[1–3] presents an insulating, quantum magnetic system of dimerized $S=1/2$ Cu^{2+} ions. Inelastic neutron scattering (INS) measurements of the elementary magnon excitations[4,5] reveal a strong dispersion in all three spatial dimensions indicative of significant interdimer interactions. The dispersion minimum gives a spin gap $\Delta_0 = 0.7$ meV, which is significantly smaller than the antiferromagnetic (AF) dimer superexchange parameter $J \approx 5$ meV. The corresponding critical field, $H_c = 5.6$ T, makes $TlCuCl_3$ one of the few known inorganic systems in which the gap may be closed by application of laboratory magnetic fields.[2] Neutron-diffraction measurements at fields $H > H_c$ revealed that a field-induced AF order in the plane normal to the applied field appears simultaneously with the uniform moment.[6] Recent INS measurements of the magnon spectra in finite fields,[7] including those exceeding H_c,[8] have provided dynamical information concerning the elementary excitations, in particular the linear Goldstone mode,[9] in the phase of field-induced magnetic order.

$TlCuCl_3$ (Fig. 1) is one member of a group of related compounds. The potassium analog $KCuCl_3$ (Refs. 1,2,10–13,7) is similarly dimerized, but has significantly weaker interdimer couplings,[14] resulting in a large spin gap of 2.6 meV. A further material in the same class, NH_4CuCl_3, has no spin gap and exhibits magnetic order with a very small moment, but also shows a complicated low-temperature structure which gives rise to magnetization plateaus only at 1/4 and 3/4 of the saturation value.[15] While the apparent increase of interdimer couplings with anion size may suggest a contribution of the anion to superexchange processes, it should be noted that the physical origin of the properties of NH_4CuCl_3 may be rather different from the other members.[16] Turning from chemical to physical pressure, Tanaka *et al.*[17] found by magnetization measurements under hydrostatic pressure that $TlCuCl_3$ has a pressure-induced magnetically ordered phase, with a very small critical pressure for the onset of magnetic order, $P_c \sim 2$ kbar. Oosawa *et al.*[18] have shown very recently by elastic neutron-scattering measurements under a pressure of 1.48 GPa that the pressure-induced ordered phase has a strong staggered moment (60% of the saturation value), again reflecting the low value of P_c. The magnetic Bragg reflections are found at reciprocal-lattice points $\boldsymbol{Q}=(0,0,2\pi)$ (following the notation of Ref. 4), as in the field-induced ordered phase of $TlCuCl_3$. The aim of the present work is to compare and contrast the field- and pressure-induced ordered phases of the system, and to provide a complete description of the static magnetization and dynamical excitations at all fields and pressures.

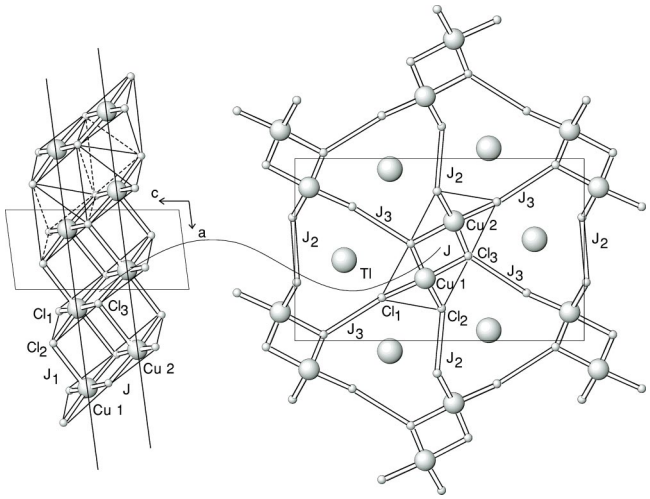

FIG. 1. Structure of $TlCuCl_3$: small circles represent Cl^- ions, medium-sized circles Cu^{2+} ions, and large circles Tl^+ ions.

The issue of coupled spin liquids and closing of the spin gap due to higher-dimensional superexchange interactions has been investigated in a wide variety of systems, many of which were found to be rather close to the quantum phase transition (QPT) to an ordered state. The Haldane chains $CsNiCl_3$ and $RbNiCl_3$ (Ref. 19) presented an early example where both static and dynamic properties could be measured. The coupled, two-leg ladder system $LaCuO_{2.5}$ (Ref. 20) was found to have sufficiently strong interladder coupling so that magnetic order could set in, whereas the coupled plaquette compound CaV_4O_9 (Ref. 21) retains a robust spin gap. While numerical simulations of appropriate models have compared the thermodynamic properties of the phases on both sides of the transition,[22] theoretical studies of these systems have concentrated in particular[23–29] on the identification of a low lying but massive longitudinal mode on the ordered side of the transition which corresponds to an amplitude fluctuation of the ordered moment. Experimental work continues to refine the observations of this type of excitation.[30]

The first system to be studied in which the spin gap could be closed by application of a magnetic field was $(CuNO_3)_2 \cdot 2.5H_2O$, whose susceptibility shows finite steps at $H=2.7$ T and 4.2 T which correspond, respectively, to the critical field and the saturation field.[31,32] Interest in this type of QPT was revived more recently by the discovery of the organometallic compound $(C_5H_{12}N_2)_2Cu_2Cl_4$.[33] This material, originally believed to have a two-leg ladder geometry, undergoes a QPT at $H_c=6.6$ T, and has been investigated quite extensively[34–36] to characterize the thermodynamic properties in the quantum critical regime. The magnetic interactions within this system are now thought to have a significantly more complex structure,[37] whose three-dimensional (3D) nature mandates a reinterpretation of earlier observations. A further recent discovery, $(C_5H_{12}N_2)_2CuBr_4$,[38] is currently believed to be a quasi-1D ladder system, and also shows an almost identical lower critical field, $H_c=6.6$ T. A considerable body of theoretical work[39–44] has analyzed the properties of this system by a variety of techniques. A particular focus of recent studies in this direction, the majority motivated by experiments on $TlCuCl_3$, has been the possibility of describing the ordered phase as a field- or pressure-driven Bose-Einstein condensation (BEC) of the triplet magnon excitations of the spin liquid,[45–48] which become massless at the QPT. In this formulation the critical exponents of thermodynamic properties such as the magnetization in the ordered phase are specified as a function of dimensionality and magnon dispersion, and allow in addition a characterization of the quantum critical regime at finite temperature. However, questions remain concerning the appropriateness and universality of this description and we will address these below.

Here we work exclusively at zero temperature to consider the field- and pressure-induced QPTs in $TlCuCl_3$ using the bond-operator technique.[49] This approach is naturally suited to the spin-liquid regime of dimerized systems[50] and has previously been developed both for coupled ladders[51] and for describing the neighboring magnetically ordered phases[28,52,53] on an equivalent footing. This analytical framework is thus uniquely applicable for a consistent discussion of static properties, and in particular of dynamical excitations, on both sides of a QPT. In Sec. II we consider the structure of $TlCuCl_3$ and deduce the parameters of the effective model for the elementary magnon excitations in zero field. Section III contains the bond-operator description of the quantum phases and phase transitions in the $TlCuCl_3$ system as a function of the field, and as such constitutes the extended version of our previous results for magnetizations and magnon excitations.[54] In Sec. IV we apply the bond-operator formulation to the pressure-induced QPT, extending the treatment of Refs. 28 and 53 to discuss in detail the phase and amplitude modes in $TlCuCl_3$, the effects of simultaneous pressure and field, and finally the magnetization at finite pressure. Section V presents a summary and conclusions.

II. MAGNETIC BAND STRUCTURE

$TlCuCl_3$ and $KCuCl_3$ appear to have the structure of a quasi-1D system of coupled spin chains. However, INS experiments on both systems at zero field reveal an elementary triplet excitation with a spin gap and strong dispersion in all three reciprocal-space directions. In this section we use a model of coupled dimers to provide a qualitative justification for the observed results in terms of superexchange interactions within the crystal structure. Although the dimer model is different from those of Refs. 4, 5, and 12, the results are perforce in close agreement.

A. Exchange pathways

The magnetic couplings between the spins, which are due to unpaired electrons in the Cu $d_{x^2-y^2}$ orbitals, are mediated by superexchange through the p orbitals of the Cl^- ions. Quantitative calculations of superexchange interactions, particularly for extended pathways, remain unfortunately beyond the scope of current understanding and computer power. Here we employ qualitative considerations of geometry and orbital overlap to provide plausibility arguments for the relevant model parameters.

Each Cu ion can be considered to be octahedrally coordinated by Cl (Fig. 1). The Cu $d_{x^2-y^2}$ orbitals lie in the basal planes of the octahedra, and the most important superexchange interaction J is that between ions in two edge-sharing octahedra. Such a pathway requires exchange through quasi-orthogonal orbitals on Cl, and if the environment is truly cubic Hund's rule dictates that the coupling is weakly ferromagnetic (FM). However, for a structure distorted away from this high symmetry, as in $TlCuCl_3$, AF exchange terms are expected to be stronger, although the edge-sharing configuration remains a weak superexchange path on the scale of the linear bonds in cuprates. Further superexchange terms in the chains (left side of Fig. 1) will of necessity involve pathways coupling to the Cu $d_{3z^2-r^2}$ orbitals, and thus will be considerably weaker than J, while interchain pathways, which have the form Cu-Cl-(Tl)-Cl-Cu (Fig. 1), should also be small. From this consideration one expects a system composed of dimers, provided by the edge-sharing octahedra, with weak interdimer coupling in all directions.

Nearest-neighbor couplings in the chainlike stack of dimer units (oriented along $\hat{a}$) are also of the edge-sharing

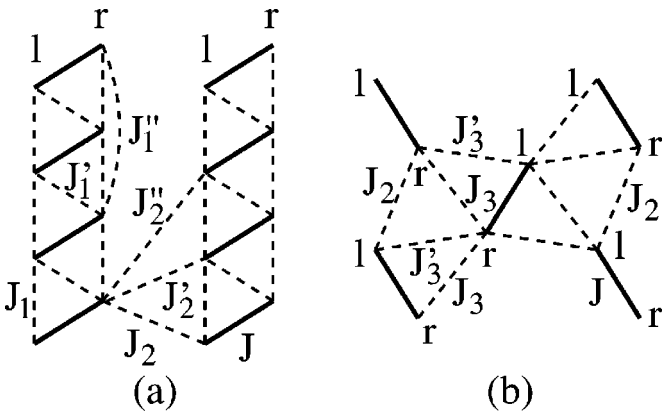

FIG. 2. Schematic representation of relevant interdimer couplings in $XCuCl_3$: (a) *a*-*c* plane and (b) *b*-*c* plane.

type between octahedra, where the edge is from basal plane to apex. Again the possibility arises from the geometry that these weak bonds may be FM. Viewing the dimers as ladder rungs, the effective ladder-leg coupling is denoted by J_1, and the asymmetrical cross coupling by J_1' [Fig. 2(a)]. Finally, the structure of the ladder legs is such that a next-neighbor Cu-Cl-Cl-Cu coupling, similar to that proposed in $CuGeO_3$, may not be excluded, and this is denoted as J_1''. A significant interchain coupling is expected only where the Cu-Cl-Cl-Cu pathway is rather direct, with bond angles not deviating widely from 180°. The dimers are oriented primarily along the *c* axis (Fig. 1), where by inspection any overlap is not especially direct and may involve parallel paths. Because the dimers are also tilted significantly along $\hat{a}$, it is possible that dimers with a separation of one or two unit cells in this direction are coupled; let J_2 denote a dimer coupling along $\hat{c}$ only, J_2' a coupling along $\hat{a}+\hat{c}$, and J_2'' a coupling along $2\hat{a}+\hat{c}$ [Fig. 2(a)]. Finally, the shortest interchain distance is that between the two inequivalent chains in the unit cell, namely, $\frac{1}{2}\hat{b}+\frac{1}{2}\hat{c}$ (Fig. 1). Here the directionality is evident from the fact that the pathway goes through the Cl ions pointing maximally up or down (relative to the *a* axis) from the dimers, indicating that this coupling J_3 should correspond to the interdimer separations $\eta\hat{a}+\frac{1}{2}\hat{b}+\frac{1}{2}\eta\hat{c}$, where $\eta=\pm 1$. The possibility remains that the couplings of the spin on one dimer to either of those on a neighboring dimer are finite, requiring a final superexchange parameter J_3' [Fig. 2(b)]; inspection of bond lengths and angles (Fig. 1) suggests that $J_3'<J_3$.

B. Model

Having argued that the properties of the system in zero field, including the spin gap, are determined largely by the dominant dimer coupling *J*, one may construct a model with this ground state using the bond-operator technique.[49] In this representation the $S=1/2$ spin degrees of freedom on each dimer, or ladder rung, are expressed by the bond operators

$$|s\rangle=s^\dagger|0\rangle=\frac{1}{\sqrt{2}}(|\uparrow\downarrow\rangle-|\downarrow\uparrow\rangle),$$

$$|t_x\rangle=t_x^\dagger|0\rangle=-\frac{1}{\sqrt{2}}(|\uparrow\uparrow\rangle-|\downarrow\downarrow\rangle),$$

$$|t_y\rangle=t_y^\dagger|0\rangle=\frac{i}{\sqrt{2}}(|\uparrow\uparrow\rangle+|\downarrow\downarrow\rangle),$$

$$|t_z\rangle=t_z^\dagger|0\rangle=\frac{1}{\sqrt{2}}(|\uparrow\downarrow\rangle+|\downarrow\uparrow\rangle), \quad (1)$$

where the arrows in each state denote the direction of the two spins, and all the states created in Eq. (1) have total (dimer) $S_z=0$. From the action of the spin operators $\mathbf{S}_l$ and $\mathbf{S}_r$ (denoting left and right sites of the dimer) on these states one may deduce[45] the correspondence

$$S_{l,r}^\alpha=\pm\frac{1}{2}(s^\dagger t_\alpha+t_\alpha^\dagger s)-i\epsilon_{\alpha\beta\gamma}t_\beta^\dagger t_\gamma, \quad (2)$$

where $\alpha,\beta,\gamma\equiv x,y,z$. The spin commutation relations for $\mathbf{S}_{l,r}$ are recovered if the singlet and triplet operators have bosonic statistics. However, the bond operators are constrained by the number of physical states available on each dimer, one singlet or one of three triplets, to obey the condition

$$s_i^\dagger s_i+\sum_{\alpha=x,y,z}t_{i,\alpha}^\dagger t_{i,\alpha}=1, \quad (3)$$

which specifies a hard-core bosonic nature.

With a view to the analysis to be presented in the subsequent sections of the system under a finite magnetic field, we introduce here the appropriate bond-operator description. The operators in Eq. (1) are not the eigenstates of an external magnetic field, and so we transform these to the operators[52]

$$t_x=\frac{1}{\sqrt{2}}(t_+ + t_-),$$

$$t_y=\frac{-1}{\sqrt{2}}i(-t_+ + t_-),$$

$$t_z=t_0, \quad (4)$$

which create the triplet states

$$t_+^\dagger|0\rangle=-|\uparrow\uparrow\rangle,$$

$$t_0^\dagger|0\rangle=\frac{1}{\sqrt{2}}(|\uparrow\downarrow\rangle+|\uparrow\downarrow\rangle),$$

$$t_-^\dagger|0\rangle=|\downarrow\downarrow\rangle. \quad (5)$$

In this basis the magnetic-field term for a dimer has the diagonal representation

$$-\boldsymbol{h}\cdot(\boldsymbol{S}_1+\boldsymbol{S}_2)=ih_z(t_x^\dagger t_y-t_y^\dagger t_x)=h(t_+^\dagger t_+-t_-^\dagger t_-), \quad (6)$$

in which $\boldsymbol{h}=g\mu_B\boldsymbol{H}$, ensuring that the operators $t^\dagger_{0,\pm1}$ reproduce the energy levels of the field eigenstates $S_z=0,\pm1$. Further, the transformation conserves particle number, and the local constraint (3) retains the form

$$s_i^\dagger s_i+\sum_{\alpha=+,0,-} t_{i\alpha}^\dagger t_{i\alpha}=1. \tag{7}$$

Following Ref. 50, transformation to the bond-operator representation yields

$$\mathcal{H}=\mathcal{H}_0+\mathcal{H}_1+\mathcal{H}_1'+\mathcal{H}_1''+\mathcal{H}_2+\mathcal{H}_2'+\mathcal{H}_2''+\mathcal{H}_3+\mathcal{H}_3', \tag{8}$$

where

$$\mathcal{H}_0=\sum_i\left[\epsilon_{is}s_i^\dagger s_i+\sum_{\alpha=+,0,-}\epsilon_{i\alpha}t_{i\alpha}^\dagger t_{i\alpha}+\mu_i\right],$$

$$\mathcal{H}_1=\frac{1}{2}J_1\sum_i\left[\mathcal{H}_{\rm st}(i,i+\hat{a}_1)+\mathcal{H}_{\rm tt}(i,i+\hat{a}_1)\right],$$

$$\mathcal{H}_1'=\frac{1}{4}J_1'\sum_i\left[-\mathcal{H}_{\rm st}(i,i+\hat{a}_1)+\mathcal{H}_{\rm tt}(i,i+\hat{a}_1)\right],$$

$$\mathcal{H}_1''=\frac{1}{2}J_1''\sum_i\left[\mathcal{H}_{\rm st}(i,i+\hat{a}_1'')+\mathcal{H}_{\rm tt}(i,i+\hat{a}_1'')\right],$$

$$\mathcal{H}_2=\frac{1}{4}J_2\sum_i\left[-\mathcal{H}_{\rm st}(i,i+\hat{a}_2)+\mathcal{H}_{\rm tt}(i,i+\hat{a}_2)\right],$$

$$\mathcal{H}_2'=\frac{1}{4}J_2'\sum_i\left[-\mathcal{H}_{\rm st}(i,i+\hat{a}_2')+\mathcal{H}_{\rm tt}(i,i+\hat{a}_2')\right],$$

$$\mathcal{H}_2''=\frac{1}{4}J_2''\sum_i\left[-\mathcal{H}_{\rm st}(i,i+\hat{a}_2'')+\mathcal{H}_{\rm tt}(i,i+\hat{a}_2'')\right],$$

$$\mathcal{H}_3=\frac{1}{4}J_3\sum_{i,\pm}\left[\mathcal{H}_{\rm st}(i,i+\hat{a}_{3\pm})+\mathcal{H}_{\rm tt}(i,i+\hat{a}_{3\pm})\right],$$

$$\mathcal{H}_3'=\frac{1}{4}J_3'\sum_{i,\pm}\left[-\mathcal{H}_{\rm st}(i,i+\hat{a}_{3\pm})+\mathcal{H}_{\rm tt}(i,i+\hat{a}_{3\pm})\right].$$

In $\mathcal{H}_0$, ϵ_{is} and $\epsilon_{i\alpha}$ denote the singlet and triplet energies in the presence of an external magnetic field directed along the z axis, and μ_i is a chemical potential emerging from the Lagrange multiplier introduced to enforce the constraint (7) on each dimer. The bond Hamiltonian $\mathcal{H}_{\rm st}(i,j)$ is specified by

$$\mathcal{H}_{\rm st}(i,j)=\sum_\alpha\left(t_{i\alpha}^\dagger t_{j\alpha}s_j^\dagger s_i+t_{i\alpha}^\dagger t_{j\bar{\alpha}}^\dagger s_i s_j+\text{H.c.}\right), \tag{9}$$

where $\alpha=+,0,-$ and $\bar{\alpha}=-,0,+$, and describes singlet-triplet interaction processes. The first two terms in Eq. (9) correspond, respectively, to triplet propagation and triplet pair creation. The triplet-triplet interaction term is given by

$$\begin{aligned}\mathcal{H}_{\rm tt}(i,j)=&\left[t_{j0}^\dagger t_{i0}(t_{i+}^\dagger t_{j+}+t_{i-}^\dagger t_{j-})+\text{H.c.}\right]\\&-\left[t_{i0}t_{j0}(t_{i+}^\dagger t_{j-}^\dagger+t_{i-}^\dagger t_{j+}^\dagger)+\text{H.c.}\right]\\&+(t_{i+}^\dagger t_{i+}-t_{i-}^\dagger t_{i-})(t_{j+}^\dagger t_{j+}-t_{j-}^\dagger t_{j-}),\end{aligned} \tag{10}$$

and encodes the possible triplet scattering processes. As in previous analyses[50,28] we have chosen to neglect terms of the form $t_{i\alpha}^\dagger t_{j\beta}^\dagger t_{j\gamma}s_i$. These three-triplet interactions vanish identically for a centrosymmetric system,[49,50] as is the case for $TlCuCl_3$ in the disordered phase, and in the ordered phase their contributions may be assumed to be small. Finally, $\hat{a}_i$ specifies the bond vectors

$$\begin{aligned}\hat{a}_1&=\hat{a},\\ \hat{a}_1''&=2\hat{a},\\ \hat{a}_2&=\hat{c},\\ \hat{a}_2'&=\hat{a}+\hat{c},\\ \hat{a}_2''&=2\hat{a}+\hat{c},\\ \hat{a}_{3\pm}&=\pm\hat{a}+\frac{1}{2}\hat{b}\pm\frac{1}{2}\hat{c},\end{aligned} \tag{11}$$

for the superexchange interactions of Fig. 2, where $\hat{a}$, $\hat{b}$, and $\hat{c}$ are unit vectors for the crystal axes. The prefactor of each term in Eq. (8) is determined by the number of bonds between dimers, and the sign of $\mathcal{H}_{\rm st}$ by whether the bond is between like (ll, rr) or unlike spins (lr).

C. Conventional bond-operator formulation

At zero field, as for all magnetic fields below the critical field H_c, the system is in the quantum disordered regime with a spin gap between the singlet and triplet states on each dimer. This situation, for which the bond-operator technique is most directly applicable, is represented by neglecting the dynamics of the singlet operator and replacing s_i everywhere by a c-number $\overline{s_i}$, corresponding to a condensate of dimer singlets. Two approaches for the treatment of the local constraint (7) in the disordered phase exist in the literature, and we begin with a brief discussion of the conventional bond-operator theory,[49] in which the chemical potential is retained explicitly. Proceeding within a mean-field approximation, the operators s_i and the site-dependent chemical potentials μ_i are replaced by uniform, global average values $\langle s_i\rangle=\overline{s}$ and $\mu_i=\mu$. These parameters are then determined self-consistently from a minimization of the total energy at fixed total boson number. The dimer energies ϵ_{is} and $\epsilon_{i\alpha}$ in $\mathcal{H}_0$ take the values

$$\epsilon_{is}=-\frac{3}{4}J-\mu,$$

$$\epsilon_{i\alpha}=\frac{1}{4}J-\alpha h-\mu, \tag{12}$$

and the self-consistent solution follows exactly the treatment of Refs. 51 and 28, which also present the situation for a system with two dimers per unit cell.

Quantum fluctuations about this dimer-singlet ground state are contained in the triplet operators $t_{i\alpha}^{\dagger}$ in Eqs. (8) and (9), and in reciprocal space are given to quadratic order by the Hamiltonian

$$\mathcal{H}=N\left(-\frac{3}{4}J\overline{s^2}-\mu\overline{s^2}+\mu\right)+\sum_{\boldsymbol{k}}\left\{\sum_{\alpha=+,0,-}\epsilon_{\boldsymbol{k}\alpha}t_{\boldsymbol{k}\alpha}^{\dagger}t_{\boldsymbol{k}\alpha}+\frac{1}{2}(\Lambda_{\boldsymbol{k}}t_{\boldsymbol{k}0}t_{-\boldsymbol{k}0}+\text{H.c.})+\frac{1}{2}\Lambda_{\boldsymbol{k}}(t_{\boldsymbol{k}+}t_{-\boldsymbol{k}-}+t_{\boldsymbol{k}-}t_{-\boldsymbol{k}+}+\text{H.c.})\right\}, \tag{13}$$

where N is the number of dimers in the system. The dispersive part of the magnon energies for the $TlCuCl_3$ system is contained in the expressions

$$\epsilon_{\boldsymbol{k}\alpha}=\frac{1}{4}J-\mu+\Lambda_{\boldsymbol{k}}-\alpha h, \tag{14}$$

$$\Lambda_{\boldsymbol{k}}=\overline{s^2}\{(J_1-\tfrac{1}{2}J_1')\cos k_x+J_1''\cos 2k_x-\tfrac{1}{2}[J_2\cos k_z+J_2'\cos(k_x+k_z)+J_2''\cos(2k_x+k_z)]+(J_3-J_3')\cos(k_x+\tfrac{1}{2}k_z)\cos\tfrac{1}{2}k_y\}, \tag{15}$$

where k_z takes values in the interval $-2\pi<k_z\leqslant 2\pi$ in order to describe the two dispersion branches corresponding to the two-sublattice system. The Brillouin zone lies between $-\pi$ and π (in units of the inverse lattice spacing) in the other two directions. Diagonalization of the Hamiltonian (13) by Bogoliubov transformation gives three modes with dispersion relations $E_{\boldsymbol{k}}+h$, $E_{\boldsymbol{k}}$, and $E_{\boldsymbol{k}}-h$, where

$$E_{\boldsymbol{k}}=\sqrt{\left(\frac{1}{4}J-\mu+\Lambda_{\boldsymbol{k}}\right)^2-\Lambda_{\boldsymbol{k}}^2} \tag{16}$$

is the dispersion relation for the field-free system. In the disordered regime the triplet modes do not change the form of their dispersion, and are merely split by the magnetic field due to the Zeeman interaction.

D. Holstein-Primakoff expansion

The alternative means of treating the global constraint is to replace the singlet operator by using the constraint itself,

$$s_i=s_i^{\dagger}=\sqrt{1-\frac{1}{N}\sum_{i,\alpha=+,0,-}t_{i\alpha}^{\dagger}t_{i\alpha}}, \tag{17}$$

which leads to the simultaneous elimination of the variable μ. Substitution of Eq. (17) into the Hamiltonian, followed by truncation at quadratic order after the expansion of the square root, is equivalent to taking $\overline{s}=1$ and $\mu=-\frac{3}{4}J$ in the formulation of the preceding subsection, and at higher fields (beyond H_c) to specifying that the condensate amplitude remains unity. With these values of $\overline{s}$ and μ the results of this approximation have exactly the form of Eqs. (13)–(16).

TABLE I. Dimer superexchange parameter J, interdimer superexchange parameters J_i, gap Δ_0, singlet condensation parameter $\overline{s}$, and chemical potential μ, determined from the bond-operator analysis of $TlCuCl_3$ and $KCuCl_3$. Values to the left in each column are obtained from the Holstein-Primakoff formulation of Sec. II D, while values in parentheses are obtained from the conventional bond-operator theory of Sec. II C. $\tilde{J}_1$ denotes the combination $2J_1-J_1'$ and $\tilde{J}_3$ the combination J_3-J_3'.

	$TlCuCl_3$	$KCuCl_3$
J/meV	5.50 (4.87)	4.22 (4.16)
$\tilde{J}_1$/meV	−0.43 (−0.41)	−0.42 (−0.48)
J_2''/meV	3.16 (3.31)	0.79 (0.75)
$\tilde{J}_3$/meV	0.91 (1.00)	0.70 (0.68)
Δ_0/meV	0.70 (0.71)	2.60 (2.65)
$\overline{s}$	1.00 (0.97)	1.00 (1.00)
$-\mu/J$	0.75 (0.86)	0.75 (0.77)

The Holstein-Primakoff approximation thus neglects quantum fluctuations to triplet dimers within the singlet condensate, and as such constitutes a stronger approximation than the approach of the preceding subsection, in which these fluctuations are included in the self-consistent determination of $\overline{s}$. The values of $\overline{s}$ obtained for the disordered phase in $TlCuCl_3$ and $KCuCl_3$ are shown in Table I, and demonstrate that the triplet fluctuations are always small. The maximal error incurred is of order 3% in this regime, while at saturation, where quantum fluctuations are completely suppressed, the condensate amplitude is in any case forced to unity. In the light of this observation, truncation at quadratic order, which is equivalent to the neglect of magnon-magnon interactions in both disordered and ordered phases, is also not a source of significant error. The superexchange parameters fitted within each of the two approaches (Table I) allow a further comparison, and are also in rather close agreement, as discussed in detail in the following subsection. Thus the Holstein-Primakoff treatment yields semiquantitative accuracy for 3D systems such as $TlCuCl_3$ and $KCuCl_3$ at low temperatures, and we will use this level of approximation in all of the analyses to follow.

E. Superexchange parameters

The zero-field dispersion relations (16) deduced from the model in Fig. 2 may be compared directly with the experimental results for $TlCuCl_3$ and $KCuCl_3$, which we take, respectively, from Refs. 4 and 12. The most characteristic features of the dispersion data for both systems are that local minima appear at both the 0 and π points in both k_x and k_z directions, and that the relative depths of these minima in $\hat{k}_x$ ($\hat{k}_z$) are exchanged between 0 and π in $\hat{k}_z$ ($\hat{k}_x$). Without attempting a systematic optimization procedure it is possible

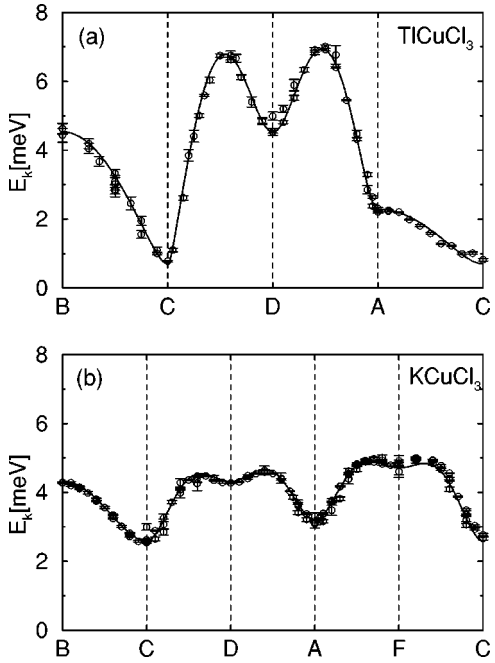

FIG. 3. (a) Magnon dispersion $E_{\boldsymbol{k}}$ for $TlCuCl_3$. The points represent experimental results measured at $T=1.5$ K, taken from Ref. 4, and the solid lines the fit using the parameters obtained within the Holstein-Primakoff formulation listed in Table I. (b) Magnon dispersion for $KCuCl_3$. Experimental data, measured at 5 K, are taken from Ref. 12, and the theoretical fit from the Holstein-Primakoff parameters of Table I. Following Ref. 4, points in reciprocal space are denoted by $B=(0,2\pi,2\pi)$, $C=(0,0,2\pi)$, $D=(0,0,0)$, $A=(\pi,0,0)$, and $F=(\pi,0,2\pi)$.

to find parameters (Table I) giving a very good account of the data. Figure 3(a) shows the calculated magnon dispersion for $TlCuCl_3$ with the data of Ref. 4 and Fig. 3(b) the dispersion for $KCuCl_3$ with the data of Ref. 12.

Under the assumption that the $\pm\hat{a}+\frac{1}{2}\hat{b}\pm\frac{1}{2}\hat{c}$ coupling is indeed dominated by J_3, the signs of the superexchange interactions are consistent with the expectation that all intersite parameters $\{J\}$ in Fig. 2 are AF. The values for $KCuCl_3$ are consistent with the results of Refs. 10, 12, and 13, with discrepancies arising from the exact formulation of the dimer description. The leading difference between $TlCuCl_3$ and $KCuCl_3$ lies in the value of the interladder coupling J_2'', which is larger for $TlCuCl_3$, and is responsible for the contrast between wide-band, small-gap and narrow-band, large-gap magnon dispersions exemplified by the two systems. We now discuss the dispersion relations and superexchange parameters in further detail.

The dominant contribution to the overall dispersion curves comes from $\tilde{J}_3$, specifically its $\cos k_x \cos\frac{1}{2}k_z$ form. Although the magnitude of this coupling is not large, its geometry enhances its importance. Separating the k_x- and k_z-dependence arising from the terms $\tilde{J}_1\equiv 2J_1-J_1'$, J_1'', J_2, J_2', and J_2'' is in principle a complex task, and tuning of these parameters would permit a very accurate fit to the measured dispersion. For the purposes of the current, unrefined fit we make use of the remarkable observation that the magnon energy in direction $[1,0,-2]$ (line AC in Fig. 3 for $TlCuCl_3$; a similar observation was made for $KCuCl_3$) is small and disperses only weakly and monotonically. In a tight-binding model this may be achieved only if the (k_x,k_z) dispersion is largely determined by the term J_2''. As in Refs. 4 and 12, we find that a good fit to all of the dispersion features can be achieved using only the parameters $\tilde{J}_1$, J_2'', and $\tilde{J}_3$, with contributions from the other parameters being negligible. From this procedure it is not possible to distinguish between the J_1 and J_1' contributions to $\tilde{J}_1$, but the result that this is negative is robust. This implies that the J_1 exchange path is closer to the FM coupling regime achieved near Cu-Cl-Cu bond angles of 90° than is the J_1' path [Fig. 1(a)]. Although it is likely that in this case both values are individually rather small, the bond-operator framework provides a simple origin for the near cancellation of two AF interactions to give a small net coupling despite the short bond lengths.

In such a scheme, the exceptionally large J_2'' required to fit the dispersion of $TlCuCl_3$ (Table I) has no immediate justification from qualitative arguments based on superexchange paths. However, it is also by no means implausible given the tilted dimer orientation within the unit cell (Fig. 2), which results in all of the bonds on this path being rather straight. However, because this coupling provides the only $\cos 2k_x$ modulation, and the only $\cos k_z$ modulation, its value is determined very accurately by its contribution to the dips away from the dispersion maxima towards the zone boundaries in both k_x and k_z directions, primarily in competition with $\tilde{J}_3$. For the strongly dimerized, 3D systems represented by both sets of parameters in Table I, these effects may only be due to competition between interactions of different periodicities, and there is no possibility of such dispersion forms being provided purely by many-body effects of the type expected in weakly coupled spin chains.[55] Such competition is ensured for the assumed dimer coupling geometry by the presence of the pathways within $\tilde{J}_3$.

As with $\tilde{J}_1$, the zero-field data alone does not permit the possibility of fitting both contributions J_3 and J_3' to the effective coupling $\tilde{J}_3$. However, because the minimum of the magnon bands is located at $(0,0,2\pi)$ in reciprocal space, one may expect (on the assumption that all couplings are AF) that $J_1'>2J_1$, whence the negative signs for the effective parameters $\tilde{J}_1$ in Table I, and that $J_3>J_3'$. One attempt has been made[5] to extract these parameters for $TlCuCl_3$ using a cluster expansion theory,[56] which returns the intersite couplings (valid for a formulation different from that of Sec. II) $J_1=0.34$ meV, $J_1'=1.70$ meV, $J_3=0.91$ meV, and $J_3'=-0.57$ meV. However, for the present purposes, namely, a focus on the ordered phases of the system under applied field and pressure, we choose to avoid the large uncertainties inherent in these estimates and proceed simply with the effective quantities $\tilde{J}_1$ and $\tilde{J}_3$, determined at zero field, in place of $\frac{1}{2}J_1$ and J_3 in Eq. (8), with $\mathcal{H}_1$ and $\mathcal{H}_3'$ set to zero. This approximation is in fact insufficient for a full treatment of the ordered phase, where the coefficients of the terms $\mathcal{H}_{\rm tt}$ have the same sign, and should no longer be nec-

essary when reliable high-field measurements become available. The resulting small deviations from quantitative accuracy which are found in reproducing the high-field magnetization (Sec. III B) imply that J_1' and J_3 are, respectively, significantly larger than J_1 and J_3'. We have thus extracted only four exchange constants (Table I) as the minimal model required to describe $TlCuCl_3$ and $KCuCl_3$, and have shown in Fig. 3 that this set provides a remarkably good account of the magnon dispersion relations in both systems. In the following sections we therefore employ this model with the parameters $(J,\tilde{J}_1,J_2'',\tilde{J}_3)$, and within the Holstein-Primakoff approximation (Sec. II D), to study field- and pressure-induced magnetic ordering in $TlCuCl_3$ and $KCuCl_3$.

We comment here that the $XCuCl_3$ structure is not magnetically frustrated; when following the dominant interactions no triangles of spins are found. The modulation of the dispersion relations arises rather from the simple fact that components of different periodicities may contribute as a consequence of the complex unit cell and coupling geometry. The lack of frustration is a very important feature for both the appearance of staggered magnetic order in an applied field and the success of the bond-operator description.

With regard to a comparison of the parameters in Table I with the results of other approaches, these are indeed rather similar to the values given in Refs. 4 [differences are due to the fact that the experimental fitting formula is linear, whereas Eq. (16) has a square-root form] and 5. The bond-operator formulation has the advantage of providing a direct justification for AF interdimer bonds J_2'' and $\tilde{J}_3$. The opposite sign of the J_2'' term found by the alternative technique is rather harder to justify on the grounds of magnitude and orbital overlap geometry. The differences between the results of Table I and those shown in Table I of Ref. 54 are due solely to the conventions chosen for the bond-operator analysis. That the magnon excitations are so well described by such a simple model indicates *a posteriori* that the qualitative assumptions made in Sec. II A concerning the relevant exchange paths are appropriate. The increase in interdimer coupling strengths observed from $KCuCl_3$ to $TlCuCl_3$, as the anion size increases, may suggest that the role of the anion in determining the superexchange parameters may depend more on its charge distribution (active participation in superexchange) than merely on its spacing effect.

In summary, $TlCuCl_3$ and $KCuCl_3$ are well described by simple models of dimerized Cu spins coupled by relatively weak superexchange interactions in all three spatial dimensions. This model may be used not only for magnon dispersion relations measured by INS, but also for the intensities of the elementary excitations, which are dominated by the dimer form factor. With these zero-field results we turn now to a treatment of the excitations in magnetic fields $H>H_c$ sufficient to close the spin gap in $TlCuCl_3$. In Sec. IV we will return to these considerations to justify our treatment of the superexchange integrals under applied hydrostatic pressure.

III. FIELD-INDUCED ORDER

In the preceeding section we have established a minimal model within the bond-operator framework which describes the ground-state and magnetic excitations of $TlCuCl_3$ and $KCuCl_3$ at zero magnetic field. In this section we will apply the same formalism to consider the evolution of the system under an applied field, with particular focus on the excitations of $TlCuCl_3$ in the experimentally accessible intermediate-field regime $H>H_c$, where the lowest-lying magnon mode is gapless.

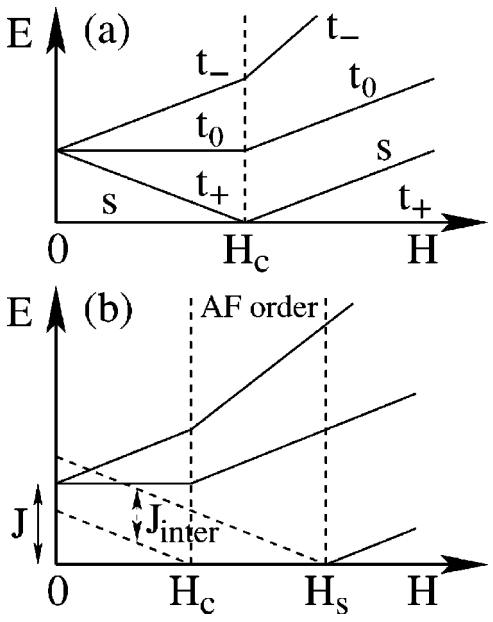

FIG. 4. Representation of field-induced order for (a) an isolated dimer and (b) interacting dimers with interdimer coupling J_{inter}.

The bond-operator formulation for ground and excited states in magnetically ordered phases was first explored for systems where the order arises as a result of increasing the superexchange interactions between low-dimensional subsystems with a spin gap.[28] In this case, all three magnon modes in the disordered phase remain degenerate as the coupling rises and the spin gap is closed, until at the quantum critical point (QCP) the three magnons become massless at the band minimum (magnetic Bragg point). On further increase of the coupling into the ordered phase, two of the magnons remain massless, corresponding to spin waves, while the third acquires a mass which increases on moving away from the QCP. This last excitation has the interpretation of a longitudinal mode, and corresponds to fluctuations in the amplitude of the order parameter, which are soft close to the QCP. This situation will be discussed further in Sec. IV in the context of the pressure-induced QPT in $TlCuCl_3$.

The situation in a magnetic field is rather different, and has been considered using bond operators for the isolated spin ladder,[52] for a pair of coupled planes,[53] and for $TlCuCl_3$ in Ref. 50. A simple understanding may be obtained by considering a single, isolated dimer with AF coupling J: at zero field the ground state is a singlet, and the threefold degenerate triplet excitations at energy $\Delta=J$ separate in an applied field due to the Zeeman interaction, as shown schematically in Fig. 4(a). At a critical field, given by $h_c\equiv\Delta$, the energy of the lowest triplet is reduced to zero, and the crossing of levels changes the ground state from singlet to triplet. Above

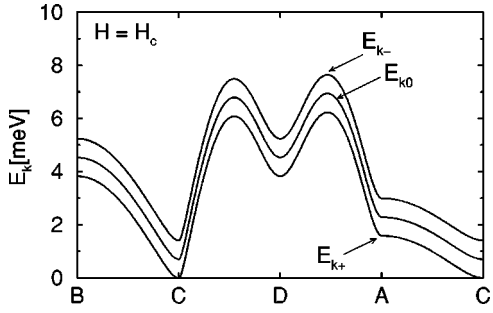

FIG. 5. Magnon dispersion for $TlCuCl_3$ at $H=H_c$ (=5.6 T), using $g=2.16$ for the g factor of $TlCuCl_3$.

H_c, the ground state is of pure triplet nature and the lowest-lying excitation is a singlet. For a set of dimers with mutual AF interactions [Fig. 4(b)], the zero-field triplet excitation modes are dispersive in reciprocal space, and the critical field H_c is defined by the value required to close the zero-field gap, at which point a single mode becomes massless.

The ground state of the ordered phase has the two essential properties that it possesses a field-induced staggered moment and has a massless excitation corresponding to the transverse fluctuations of this moment. The appropriate description of this phase is a linear combination with the singlet of the lowest- and highest-lying triplet states,[54] which corresponds to the choice of a mean field for the staggered moment, whence the transformation in Holstein-Primakoff formulation returns the excitations of the ordered phase. We note here that the conventional bond-operator treatment (Sec. II C) may lose consistency in the description of these excitations because higher-order interactions between triplets are contained in an uncontrolled manner. The coefficients of the ground-state singlet-triplet admixture change continuously with the applied field until the upper critical field H_s, where all spins are aligned. Beyond H_s, the ground state has pure triplet character (Fig. 4) and three excited modes of the strong-field regime are all massive, as expected for a field-aligned antiferromagnet.

A. Disordered phase

Henceforth we adopt the notation J_1 for $\tilde{J}_1$, J_2 for J_2'', and J_3 for $\tilde{J}_3$. As in Sec. II C, the dispersion relations for the triplet magnons of the disordered phase are given by

$$E_{\boldsymbol{k}\alpha}=\sqrt{J^2+2J\epsilon_{\boldsymbol{k}}}-\alpha h, \tag{18}$$

$$\epsilon_{\boldsymbol{k}}=-\frac{1}{2}J_1\cos k_x-\frac{1}{2}J_2\cos(2k_x+k_z)$$

$$+J_3\cos(k_x+\tfrac{1}{2}k_z)\cos\frac{1}{2}k_y, \tag{19}$$

and are shown in Fig. 5 for the critical field h_c, although a qualitatively identical picture is obtained for all fields $h\leqslant h_c$. We emphasize that the lowest mode retains its quadratic shape at the band minimum (cf. Sec. IV) even at h_c, while beyond this, as we will demonstrate below, an additional linear component arises.

The nature of the three magnon modes in the disordered phase may be understood as follows. The wave function of the lowest triplet mode, $E_{\boldsymbol{k}+}$, can be approximated by a linear combination of singlets and triplets on each dimer bond,

$$\psi_i\sim\frac{1}{\sqrt{2}}u(|\uparrow\downarrow\rangle-|\uparrow\downarrow\rangle)-ve^{i(\boldsymbol{k}\cdot\boldsymbol{r}_i-E_{\boldsymbol{k}+}t)}|\uparrow\uparrow\rangle, \tag{20}$$

where u is a coefficient of order unity and v is small and real. The expectation values of the spin operator components at a given dimer i in the state (20) are

$$\langle S_{l,x}\rangle_i=-\langle S_{r,x}\rangle_i\sim\frac{1}{2}uv\cos(\boldsymbol{k}\cdot\boldsymbol{r}_i-E_{\boldsymbol{k}+}t),$$

$$\langle S_{l,y}\rangle_i=-\langle S_{r,y}\rangle_i\sim-\frac{1}{2}uv\sin(\boldsymbol{k}\cdot\boldsymbol{r}_i-E_{\boldsymbol{k}+}t),$$

$$\langle S_{l,z}\rangle_i=\langle S_{r,z}\rangle_i\sim\frac{1}{2}v^2, \tag{21}$$

from which it is evident that the mode possesses a very small, uniform, static magnetic moment parallel to the field, and thus gains Zeeman energy. Perpendicular to the field there is also a finite magnetic moment, which fluctuates in both space and time with characteristic wave vector $\boldsymbol{k}$ and energy $E_{\boldsymbol{k}+}$, and is staggered (spins l and r oppositely aligned) because of the AF intradimer coupling J. Similar considerations for the mode $E_{\boldsymbol{k}-}$ reveal that the uniform magnetic moment is directed antiparallel to the field, leading to a higher Zeeman energy. Finally, the $E_{\boldsymbol{k}0}$ mode has no magnetization perpendicular to the field, although it does possess a moment parallel to the field with modulation wave vector $\boldsymbol{k}$, and so its energy does not change with field. For $H<H_c$, the energies of these modes are positive, meaning that the spin structure associated with the magnons is very weak and fluctuating. We stress that the sum of the magnetization components remains zero in the disordered phases, which can be considered as a consequence of quantum fluctuations which act to restore the O(3) symmetry of the field-free system.

We note again that an increase in the applied field leads to a shift in mode energies without changing the shape of their zero-field dispersion, until the lowest mode ($\alpha=+$) becomes soft at $\boldsymbol{Q}=(0,0,2\pi)$. This determines both the critical field,

$$h_c=g\mu_{\mathrm{B}}H_c=\sqrt{J^2-J(J_1+J_2+2J_3)}, \tag{22}$$

and the spin structure of the lowest-lying mode, given by $\boldsymbol{k}=\boldsymbol{Q}$, which corresponds to the static spin configuration in the field-induced ordered phase. One may conclude that a $TlCuCl_3$ system of classical spins would favor AF order to minimize simultaneously all intersite interaction terms. By contrast, for the quantum system the strong AF intradimer interaction J favors dimer-singlet formation, and the AF spin structure cannot be the ground state for $H<H_c$. However, the incipient, long-ranged AF spin order is reflected in the

structure of the lowest-lying magnon excitation, which is minimal at $\boldsymbol{k}=\boldsymbol{Q}$. As the magnetic field is increased, the lowest mode is lowered progressively until H_c, where dimer-singlet formation is no longer sufficient to cause an ordered phase, the symmetry of the system is lowered to O(2), and the onset of real uniform and staggered magnetization components is observed. For the magnon excitations in the ordered regime, the instability is signaled by the lowest mode becoming negative within the formulation of this subsection. We turn now to a consistent description of all of these phenomena in the ordered phase ($H>H_c$).

B. Ordered phase ($H_c \leqslant H \leqslant H_s$)

1. Magnon excitations

In the intermediate-field regime, the ground state of each dimer can be considered as a partially polarized FM configuration. It is important to note that there is no explicit AF component in the dimer ground state, and that the ordering emerges only from closing of the gap to the lowest magnon branch at $\boldsymbol{k}=\boldsymbol{Q}$. In the bond-operator formulation, this ordered ground state is represented[53,54] in the basis of Eq. (4) by finite expectation values $\bar{s}$, $\bar{t}_+$, and $\bar{t}_-$ of these singlet and triplet operators. The component of the highest-lying triplet mode in the ground-state condensate may appear counterintuitive, and was neglected in a number of approximate treatments.[41,52] However, the presence of terms of the form $t_{i+}^\dagger t_{j-}^\dagger s_j s_i$ in the transformed Hamiltonian of Eq. (9) makes clear that a finite component of this state is required in the consistent condensate.

Following the treatment of the preceding sections, the linear combination of operators appropriate for the ground-state mode is taken as the condensate, and the orthogonal mode containing a singlet component describes its gapless phase fluctuations. For a full description of the ordered regime we perform the transformation[53]

$$
\begin{aligned}
a_i &= u s_i + v(f e^{i\boldsymbol{Q}\cdot\boldsymbol{r}_i} t_{i+} + g e^{i\boldsymbol{Q}\cdot\boldsymbol{r}_i} t_{i-}),\\
b_{i+} &= u(f t_{i+} + g t_{i-}) - v e^{i\boldsymbol{Q}\cdot\boldsymbol{r}_i} s_i,\\
b_{i0} &= t_{i0},\\
b_{i-} &= f t_{i-} - g t_{i+},
\end{aligned}
\tag{23}
$$

in which the $\boldsymbol{k}$-independent coefficients u, v, f, and g arise from successive unitary transformations. The conditions $u^2+v^2=1$ and $f^2+g^2=1$ dictate that $u=\cos\theta$, $v=\sin\theta$, $f=\cos\phi$, and $g=\sin\phi$, with θ and ϕ the two independent variables required to specify the condensate.

As above, the operator a_i is treated as a uniformly condensed mean-field parameter,

$$
a_i \rightarrow \bar{a}. \tag{24}
$$

Because the two unitary transformations conserve particle number, the global constraint may be reduced in the Holstein-Primakoff representation to

$$
\bar{a} = \sqrt{1 - \frac{1}{N} \sum_{\boldsymbol{k},\alpha=+,0,-} b_{\boldsymbol{k}\alpha}^\dagger b_{\boldsymbol{k}\alpha}}. \tag{25}
$$

We emphasize again the participation of the highest triplet mode (t_-) in the condensate, as a consequence of the triplet pair-creation processes in $\mathcal{H}_{\rm st}$, Eq. (9). The linear combination of singlet and triplets in the condensate $\bar{a}$ yields a staggered magnetization perpendicular to the field, whose order is given by the wave vector $\boldsymbol{Q}$.

Using the transformed operators (23), and with replacement of the condensate parameter using the global constraint of Eq. (25), the Hamiltonian (8) is reexpressed to quadratic order in the b operators in the form

$$
\mathcal{H} = O(b^0) + O(b^1) + O(b^2), \tag{26}
$$

in which the classical part at zeroth order is given by

$$
\begin{aligned}
O(b^0) = N\{&(\epsilon_+ f^2 + \epsilon_- g^2) v^2 - \epsilon_{\boldsymbol{Q}}[-u^2 v^2 (1+2fg)\\
&+ \tfrac{1}{2} v^4 (f^2-g^2)^2]\},
\end{aligned}
\tag{27}
$$

where

$$
\epsilon_\alpha = J - \alpha h \qquad (\alpha = \pm), \tag{28}
$$

$$
\epsilon_{\boldsymbol{Q}} = -(\tfrac{1}{2} J_1 + \tfrac{1}{2} J_2 + J_3). \tag{29}
$$

The terms at linear order may be written as

$$
\begin{aligned}
O(b^1) = uv(a_0^\dagger b_{\boldsymbol{Q}+} + \text{H.c.})\{&\epsilon_+ f^2 + \epsilon_- g^2\\
&+ \epsilon_{\boldsymbol{Q}}[(u^2-v^2)(1+2fg) - v^2 (f^2-g^2)^2]\}\\
&+ uv(a_0^\dagger b_{\boldsymbol{Q}-} + \text{H.c.})[(-\epsilon_+ + \epsilon_-) fg\\
&+ \epsilon_{\boldsymbol{Q}}(u^2 + 2fgv^2)(f^2-g^2)],
\end{aligned}
\tag{30}
$$

and the requirement that this sum be zero fixes the parameter choice (θ,ϕ), which also minimizes $O(b^0)$. The equations determining the two unitary transformations are then given by

$$
\begin{aligned}
\epsilon_+ f^2 + \epsilon_- g^2 &= -\epsilon_{\boldsymbol{Q}}[(u^2-v^2)(1+2fg) - v^2 (f^2-g^2)^2],\\
(-\epsilon_+ + \epsilon_-) fg &= -\epsilon_{\boldsymbol{Q}}(u^2 + 2fgv^2)(f^2-g^2).
\end{aligned}
\tag{31}
$$

The field dependence of the coefficients u^2, v^2, f^2, and g^2 is shown in Fig. 6 for the parameters of both $KCuCl_3$ and $TlCuCl_3$. Below the critical field ($H<H_c$), the ground state is a pure singlet condensate specified by $u=1$, $v=0$, $f=1$, and $g=0$, i.e., by the angles $(\theta,\phi)=(0,0)$. Precisely at the critical field, where $u=1$ and $v=0$ ($\theta=0$), g takes on a finite value while $f<1$. In the intermediate regime, θ then changes continuously from 0 to $\pi/2$. Except for the parameters of $TlCuCl_3$ and for fields close to H_c, ϕ remains small, reflecting the fact that mixing of the upper and lower triplet modes is not generally strong. Finally, above the saturation field ($H \geqslant H_s$), the ground state becomes a pure condensate of the lowest triplet, which is described by $u=0$, $v=1$, $f=1$, and $g=0$, or by $(\theta,\phi)=(\pi/2,0)$. The critical field is determined exactly as

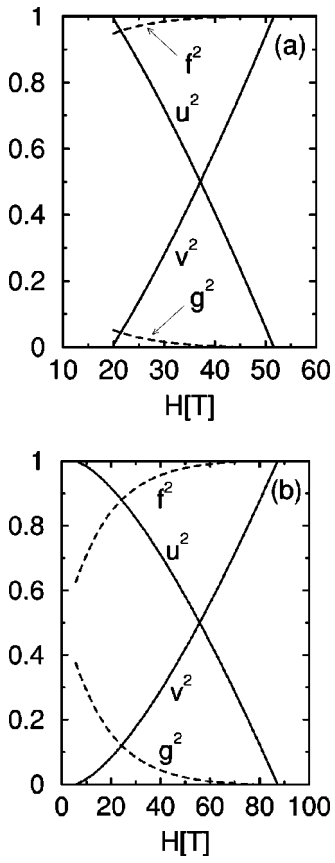

FIG. 6. Magnetic-field dependence of the coefficients u^2, v^2, f^2, and g^2 for (a) $KCuCl_3$ and (b) $TlCuCl_3$.

$$h_c = g\mu_B H_c = \sqrt{J^2 - J(J_1 + J_2 + 2J_3)}, \tag{32}$$

which coincides with the soft-mode condition (22) in the low-field regime. For $TlCuCl_3$ ($KCuCl_3$), the parameters of Table I give a critical field $H_c = 5.6$ T (19.6 T), consistent with the measured value.[2] The saturation field is determined by the condition

$$h_s = g\mu_B H_s = J + J_1 + J_2 + 2J_3 \tag{33}$$

required to overcome all of the AF bonds to a single spin.

The spin excitations in the ordered phase are described by the quadratic term in Eq. (26),

$$O(b^2) = \mathcal{H}_0 + \mathcal{H}_\pm , \tag{34}$$

where

$$\mathcal{H}_0 = \sum_{\boldsymbol{k}} \left[\epsilon_{\boldsymbol{k}0} b^\dagger_{\boldsymbol{k}0} b_{\boldsymbol{k}0} + \frac{1}{2}(\Delta^\dagger_{\boldsymbol{k}0} b_{\boldsymbol{k}0} b_{-\boldsymbol{k}0} + \text{H.c.}) \right] \tag{35}$$

and

$$\mathcal{H}_\pm = \sum_{\boldsymbol{k}} \Big[\epsilon_{\boldsymbol{k}+} b^\dagger_{\boldsymbol{k}+} b_{\boldsymbol{k}+} + \epsilon_{\boldsymbol{k}-} b^\dagger_{\boldsymbol{k}-} b_{\boldsymbol{k}-} + (\epsilon_{\boldsymbol{k}\pm} b^\dagger_{\boldsymbol{k}+} b_{\boldsymbol{k}-} + \text{H.c.}) + \frac{1}{2}(\Delta^\dagger_{\boldsymbol{k}+} b_{\boldsymbol{k}+} b_{-\boldsymbol{k}+} + \text{H.c.}) + \frac{1}{2}(\Delta^\dagger_{\boldsymbol{k}-} b_{\boldsymbol{k}-} b_{-\boldsymbol{k}-} + \text{H.c.}) + (\Delta^\dagger_{\boldsymbol{k}\pm} b_{\boldsymbol{k}+} b_{-\boldsymbol{k}-} + \text{H.c.}) \Big]. \tag{36}$$

For continuity of presentation, the expressions for $\epsilon_{\boldsymbol{k}i}$ and $\Delta_{\boldsymbol{k}i}$ are given in the Appendix [Eqs. (A1) and (A3)]. We note that on setting $(\theta, \phi) = (0,0)$ the Hamiltonian [Eqs. (27) and (34)] reduces to that of the disordered phase given in Eq. (13) with $\bar{s} = 1$ and $\mu = -\frac{3}{4}J$.

The $O(b^2)$ terms in Eq. (34) are diagonalized by two separate Bogoliubov transformations which yield the energies of the collective modes of the condensate. Because the triplet b_{k0} does not mix with the other two modes, $\mathcal{H}_0$ is diagonalized easily to give

$$E_{\boldsymbol{k}0} = \sqrt{\epsilon^2_{\boldsymbol{k}0} - \Delta^2_{\boldsymbol{k}0}}, \tag{37}$$

which describes the middle magnon branch in the ordered phase. $\mathcal{H}_\pm$ is diagonalized by the transformation

$$\alpha^m_{\boldsymbol{k}} = u^m_{\boldsymbol{k}+} b_{\boldsymbol{k}+} + u^m_{\boldsymbol{k}-} b_{\boldsymbol{k}-} + v^m_{\boldsymbol{k}+} b^\dagger_{-\boldsymbol{k}+} + v^m_{\boldsymbol{k}-} b^\dagger_{-\boldsymbol{k}-}, \tag{38}$$

where $m = 1,2$ denotes the two modes corresponding to each value of $\boldsymbol{k}$, whence

$$\mathcal{H}_\pm = \sum_{\boldsymbol{k}m} E^m_{\boldsymbol{k}} \alpha^{m\dagger}_{\boldsymbol{k}} \alpha^m_{\boldsymbol{k}} . \tag{39}$$

$E^m_{\boldsymbol{k}}$ and $\alpha^m_{\boldsymbol{k}}$ are then the eigenvalue and eigenvector for the mode of branch m, and are related by the equation

$$\begin{pmatrix} \epsilon_{\boldsymbol{k}+} & -\Delta_{\boldsymbol{k}+} & \epsilon_{\boldsymbol{k}\pm} & -\Delta_{\boldsymbol{k}\pm} \\ \Delta_{\boldsymbol{k}+} & -\epsilon_{\boldsymbol{k}+} & \Delta_{\boldsymbol{k}\pm} & -\epsilon_{\boldsymbol{k}\pm} \\ \epsilon_{\boldsymbol{k}\pm} & -\Delta_{\boldsymbol{k}\pm} & \epsilon_{\boldsymbol{k}-} & -\Delta_{\boldsymbol{k}-} \\ \Delta_{\boldsymbol{k}\pm} & -\epsilon_{\boldsymbol{k}\pm} & \Delta_{\boldsymbol{k}-} & -\epsilon_{\boldsymbol{k}-} \end{pmatrix} \begin{pmatrix} u^m_{\boldsymbol{k}+} \\ v^m_{\boldsymbol{k}+} \\ u^m_{\boldsymbol{k}-} \\ v^m_{\boldsymbol{k}-} \end{pmatrix} = E^m_{\boldsymbol{k}} \begin{pmatrix} u^m_{\boldsymbol{k}+} \\ v^m_{\boldsymbol{k}+} \\ u^m_{\boldsymbol{k}-} \\ v^m_{\boldsymbol{k}-} \end{pmatrix}. \tag{40}$$

This equation has four eigenvalues, of which two are positive, and we define the smaller of these as $E^+_{\boldsymbol{k}}$, the dispersion relation of the lowest magnon mode, while the larger is defined as $E^-_{\boldsymbol{k}}$ for the highest mode. By the nature of the problem, the other two eigenvalues are $-E^+_{\boldsymbol{k}}$ and $-E^-_{\boldsymbol{k}}$. In the disordered phase, $\epsilon_{\boldsymbol{k}\pm} = 0 = \Delta_{\boldsymbol{k}+} = \Delta_{\boldsymbol{k}-}$, and Eq. (40) reduces to a 2×2 matrix form.

In the ordered phase above H_c, the mode $E_{\boldsymbol{k}+}$ is always massless at the band minimum, $\boldsymbol{Q}$, and develops a linear dependence on $\boldsymbol{k}$ (in all three directions in reciprocal space) in the vicinity of this point [Fig. 7(a)]. This branch is the Goldstone mode, which arises from the fact that rotation of the staggered moment about the axis of broken symmetry (the field axis) does not change the energy of the system. It is the staggered magnetic order induced perpendicular to the applied magnetic field which breaks rotational symmetry around the field axis. Mathematically, rotations of the in-

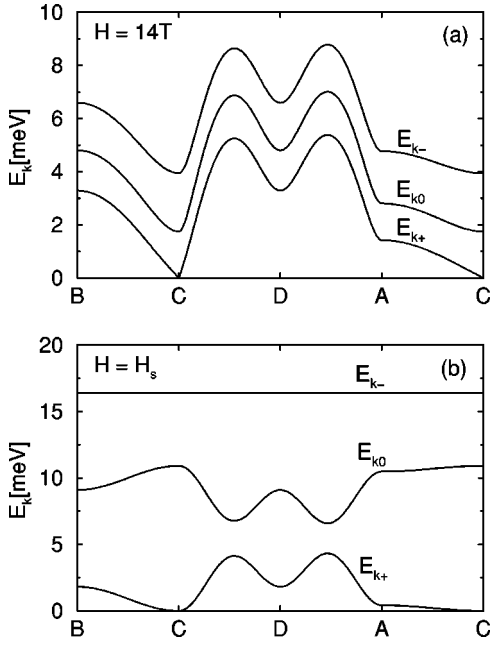

FIG. 7. Dispersion of the three magnon modes in $TlCuCl_3$ at (a) $H=14$ T$>H_c$ (cf. Ref. 9) and (b) the saturation field $H=H_s$.

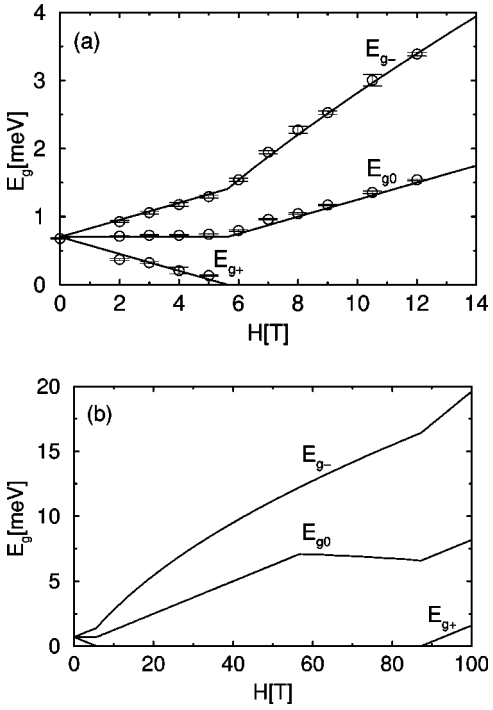

FIG. 8. Field dependence of the energy gaps for the three magnon modes in $TlCuCl_3$. (a) Points are data from the INS experiment of Ref. 8, solid lines are the theoretical fit using the zero-field parameters of Table I. (b) Field-dependence at high fields, using $g=2.16$ as the g factor of $TlCuCl_3$ (Ref. 8).

duced moment are realized by changing the phase of f and g in Eq. (23) ($f\rightarrow e^{-i\chi}f$, $g\rightarrow e^{i\chi}g$, where χ is the rotation angle), and the invariance of the expressions under this transformation determines the gapless nature of the Goldstone mode. The remaining modes in Fig. 7(a) show that for fields close to H_c the overall shape of the dispersion relations is not strongly affected by the presence of the field while the field remains small on the scale of the mode energies $E_{\boldsymbol{k}}$.

The field-dependence of magnon dispersion relations may be characterized up to high fields using the expressions obtained for $E_{\boldsymbol{k}+}$, $E_{\boldsymbol{k}0}$, and $E_{\boldsymbol{k}-}$ with the zero-field parameters of Table I. Only in the disordered phase ($H\leqslant H_c$) does the magnon dispersion not change its shape, with a simple linear splitting of the three branches developing due the Zeeman interaction until the energy gap of the lowest mode is reduced to zero at $H=H_c$. Above the critical field, the gap for $E_{\boldsymbol{k}+}$, the Goldstone mode of the ordered phase, remains zero, as a consequence of which the gaps of the higher modes, E_{g0} and E_{g-}, show an abrupt increase in slope at H_c [Fig. 8(a), cf. Fig. 4]. The results of the bond-operator theory (solid lines) show quantitative agreement with the experimental measurements obtained by INS.[8]

Figure 8(b) shows the predicted field dependence of the gaps for high fields: while E_{g-} has monotonically increasing behavior all the way to and beyond H_s, the gap E_{g0} of the middle branch first increases with field, but then decreases until H_s. This behavior is related to the position in the Brillouin zone of dispersion minimum, which is determined largely by the $\epsilon_{\boldsymbol{k}0}$ term in the Appendix. As the magnetic field is raised, the sign of the dispersive component $\epsilon_{\boldsymbol{k}}$ changes on passing through the field at which $u^2=v^2$, which for the parameters of $TlCuCl_3$ corresponds to 55 T [Fig. 6(b)]. Below this value, where $u^2>v^2$, the minimum is at $\boldsymbol{Q}$, while for fields close to 55 T ($u^2\simeq v^2$) the dispersion becomes flat. Above this field ($u^2<v^2$) the minimum moves from $\boldsymbol{Q}$ to a point in the middle of the zone, as shown for the branch $E_{\boldsymbol{k}0}$ in Fig. 7(b), and E_{g0} then decreases with field until saturation. Finally, at $H=H_s$, the $\boldsymbol{k}$ dependence of the lowest mode, $E_{\boldsymbol{k}+}$, becomes quadratic again in the vicinity of $\boldsymbol{Q}$ [Fig. 7(b)] as a gap opens to the lowest mode of the fully saturated ferromagnet [Fig. 8(b)]. For $H>H_s$ (see below), the magnon modes decouple, the condensate has pure triplet character and the lowest excitation mode is a pure singlet whose gap grows linearly with the field, as do E_{g0} and (with a slope greater by a factor of two) E_{g-}. The evolution with field of the shape of the dispersion relations through the ordered phase is illustrated by Fig. 7, where it is clear that the lower branch changes rather little, the upper branch becomes progressively narrower until it is completely nondispersive at H_s, and the middle branch is inverted as discussed above.

2. Magnetization

The theoretical framework also gives direct access to the average magnetization of the dimers in the ordered-phase condensate. We denote by M_z the magnetization parallel to the field, whose normalized value is

$$M_z=\frac{1}{N}\sum_i \langle t_{i+}^\dagger t_{i+}-t_{i-}^\dagger t_{i-}\rangle, \tag{41}$$

and by M_{xy} the perpendicular (staggered) magnetization,

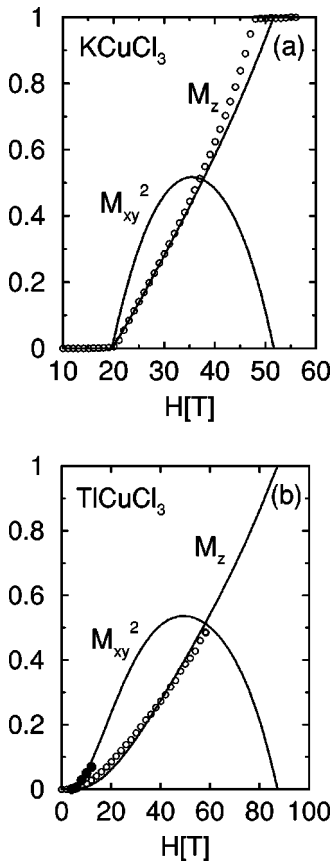

FIG. 9. (a) Normalized magnetization curves for $KCuCl_3$. Open circles are experimental data for M_z measured at $T=1.3$ K (Ref. 10). The theoretical fits are made using $g=2.29$ as the g factor for $KCuCl_3$ (Ref. 10). (b) Normalized magnetization curves for $TlCuCl_3$. Open circles are experimental data for M_z measured at $T=1.3$ K (Ref. 57), and closed circles are data for M_{xy} measured at $T=0.2$ K (Ref. 6). The theoretical fits are made using the same g factor for $TlCuCl_3$ as in Fig. 8.

$$M_{xy}=\frac{1}{N}\sum_i e^{i\mathbf{Q}\cdot\mathbf{r}_i}\langle S_{ilx}-S_{irx}\rangle$$

$$=\frac{1}{N}\sum_i e^{i\mathbf{Q}\cdot\mathbf{r}_i}\langle s_i^\dagger(t_{i+}+t_{i-})+\text{H.c.}\rangle, \qquad (42)$$

where i labels the dimers and $\langle\cdots\rangle$ signifies an expectation value calculated using the operators $\alpha_{\mathbf{k}}^m$ in Eq. (38). The mean-field magnetizations, normalized to their values at saturation are given by

$$M_z=v^2(f^2-g^2), \qquad (43)$$

$$M_{xy}=\sqrt{2}uv(f+g). \qquad (44)$$

These expressions correspond to $\overline{a^2}$ contributions, and are supplemented by terms of the form $\alpha_{\mathbf{k}}\alpha_{\mathbf{k}}^\dagger$, which correspond to quantum corrections due to magnon excitations. Both contributions are shown in Figs. 9(a) and 9(b), but the quantum corrections are found to be small, presumably as a result of the three-dimensionality of the $KCuCl_3$ and $TlCuCl_3$ systems. In both cases the square of the staggered moment (M_{xy}^2) shows a linear field dependence close to H_c and to H_s, indicating that $M_{xy}\sim\sqrt{H-H_c}$ as expected from a mean-field description.

For $KCuCl_3$, the magnetization parallel to the field (M_z) is almost perfectly linear in H [Fig. 9(a)], in good agreement with experiment.[10] If one neglects the upper triplet mode (t_-) in the condensate specified by Eq. (23), M_z would be completely linear in H, and because all interdimer interactions are small (Table I), $KCuCl_3$ is close to this limit. By contrast, the interladder interaction J_2 is considerably larger for $TlCuCl_3$, where mixing into the condensate of the t_- mode, mediated primarily by interactions of the type $t_+^\dagger t_-^\dagger ss$, is significant. This point can be seen clearly by comparing Figs. 6(a) and 6(b), where the value of g^2 is considerably larger for $TlCuCl_3$ than for $KCuCl_3$ in the vicinity of H_c. Physically, the presence of the highest triplet in the condensate costs Zeeman energy, which leads to a suppression of v, and consequently M_z is reduced near H_c for $TlCuCl_3$. This causes a significant deviation (due in fact to higher powers in $H-H_c$) from purely linear field dependence, as illustrated in Fig. 9(b), which is again in very good agreement with the observed form.[2] This result emphasizes the importance of including the t_- triplet in a consistent description of the ground state, which is required to account for the difference between the magnetization curves of $TlCuCl_3$ and $KCuCl_3$.

C. Saturated phase ($H\geqslant H_s$)

In the high-field regime the spins are fully polarized. In the notation of Sec. III B, the saturated phase is described by $(\theta,\phi)=(\pi/2,0)$ in the Hamiltonian of Eq. (26), which specifies that the ground state becomes a pure condensate of the lowest triplet (t_+ in the notation of Sec. III A). This phase is characterized by a complete decoupling of the triplet modes, by a finite energy gap to the lowest mode, which corresponds to an excitation from the triplet ground state to a singlet, and by the fact that the highest triplet mode becomes dispersionless [Fig. 7(b)]. In this regime the interaction term $\mathcal{H}_{\text{tt}}$ between the lowest and highest triplet branches in Eq. (10) becomes an on-site potential term for t_- magnons, and does not assist their propagation, so there is no first-order hopping process for this branch. A possible second-order process exists for propagation of the upper triplet by creation of two singlets in a virtual process due to the term $s_i^\dagger s_j^\dagger t_{j+}t_{i-}$ in $\mathcal{H}_{\text{st}}$. The quantitative effect of this term on the dispersion $E_{\mathbf{k}-}$ is expected to be very small, but the process may also have a qualitative role in mediating the decay of t_- magnons into two singlet modes (bearing in mind the triplet nature of the condensate). With energy and momentum conservation specified according to

$$E_{\mathbf{k}-}=\sum_{\mathbf{q}}(E_{\mathbf{k}+\mathbf{q}+}+E_{\mathbf{k}-\mathbf{q}+}), \qquad (45)$$

this may lead to a finite lifetime for the highest triplet excitations. We note also that this process is possible for fields $H_c\leqslant H\leqslant H_s$, and provides one reason for which the upper magnon mode may become broad at high magnetic fields.

IV. PRESSURE-INDUCED ORDER

In Sec. III we have discussed field-induced magnetic order in a quantum spin system, which can be understood qualitatively as the consequence of the lowering of one of the triplet modes by the applied magnetic field to the point where it becomes soft, and the ordered phases is favored. Another way in which the magnon modes may soften, causing the onset of magnetic order, is by increasing the interdimer interactions, broadening the magnon band. The application of pressure is expected to have just this effect, and for the small-gap system $TlCuCl_3$ this type of pressure-induced AF order was found recently by Oosawa *et al.*[18] in neutron-diffraction experiments conducted under a fixed hydrostatic pressure $P=1.48$ GPa.

As noted in Sec. III, this type of ''pressure-induced'' magnetic QPT provided the first application of the bond-operator formulation to ordered phases.[28] In the disordered phase the three magnon modes are degenerate at $H=0$ for all couplings, including at the QCP where they are gapless at the wave vector $\boldsymbol{Q}$ characterizing the incipient magnetic order. The excitations of the ordered AF consist of two spin waves, which are the conventional phase modes (Goldstone modes) of the ordered moment, and a third which corresponds to its amplitude fluctuations and is generally not relevant for the low-energy dynamics, but may become low-lying close to the QCP.[28] The ordered phase is described in the bond-operator approach by a condensation of one of the triplet operators, conventionally taken as $t_z^\dagger$ in Eq. (1), and in Ref. 28 this was treated as a separate condensate in order to obtain an effective description of the ordered phase close to the QCP.

A complete account of the changes to the superexchange interactions caused by the application of a hydrostatic pressure would require a detailed structural investigation of the alterations to bond lengths and angles. Such a study lies beyond the scope of the current analysis, the aim of which is to characterize the changes in physical properties through the QPT. We thus employ qualitative arguments based on the considerations of Sec. II for the probable evolution of the coupling constants in the $XCuCl_3$ structure, and use this as the foundation for a plausible model.

The structural unit composed of $CuCl_6$ octahedra is not expected to undergo significant changes except at rather high pressures, and so we assume here that the dimer coupling J is unaltered. The leading effects of hydrostatic pressure are expected to be a small longitudinal compression of the ladder units, and, due to the absence of strong covalent bonds in the transverse directions, a somewhat larger reduction in their separation. These changes generally involve small reductions in bond lengths and more significant distortions of the bond angles. Considering next the effective interdimer coupling $\tilde{J}_1=2J_1-J_1'$ (in the notation of Sec. II), any small increase in ladder-leg coupling J_1 is likely to be offset to a considerable extent by similar changes in the diagonal coupling J_1', so we will also neglect the pressure-induced alteration of this parameter in the following simplified treatment. The leading pressure effects are thus expected to involve the alteration of the parameters J_2' and J_3, both of which are determined by Cu-Cl-Cl-Cu pathways, although the latter may also have contributions from the X^+ ion. We assume (based on the experimental observation of the QPT) that J_2 and J_3 increase with the pressure P. For the functional form of this increase, the exact dependence of superexchange interactions on bond lengths and angles remains a topic active research, and in the absence of structural data under pressure we will attempt to fit this form with minimal assumptions. We take the interladder interactions to change with applied pressure according to

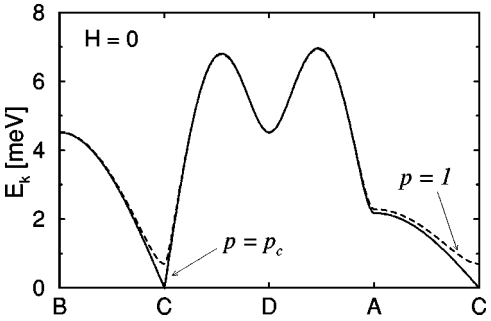

FIG. 10. Threefold degenerate triplet magnon dispersion at zero field. Dashed and solid lines correspond, respectively, to atmospheric ($p=1$) and critical ($p=p_c\simeq 1.018$) pressures.

$$J_2(P)=p(P)J_2,$$

$$J_3(P)=p(P)J_3, \tag{46}$$

where $p(P)$ is a dimensionless function of the real pressure P and the values of J_2 (J_2'') and J_3 ($\tilde{J}_3$) at $p=1$ are listed in Table I. We begin by analyzing the situation where the interladder interactions are simply increased by a factor p, and then discuss the experimental determination of the function $p(P)$.

A. No magnetic field

With a view to the simultaneous application of field and pressure (below), we discuss the pressure-induced QPT using the triplet operators t_+, t_0, and t_-, Eqs. (4), which were introduced for the field-induced QPT, rather than in the ''natural'' basis of operators t_x, t_y, and t_z, Eqs. (1). In the absence of a magnetic field, the magnon dispersion in the disordered phase is given by Eq. (16) with $h=0$, and the single branch is triply degenerate. The dispersion, shown at atmospheric pressure by the dashed line in Fig. 10 (cf. Fig. 3), is given by

$$E_{\boldsymbol{k}}=\sqrt{J^2+2J\epsilon_{\boldsymbol{k}}}, \tag{47}$$

where $\epsilon_{\boldsymbol{k}}$ is defined in Eq. (19) but with J_2 and J_3 now given by Eq. (46). As pressure is increased, the maximal positive and negative values of $\epsilon_{\boldsymbol{k}}$ are enhanced, the bandwidth increases and the dispersion minimum (spin gap) decreases. It is clear from Fig. 10 that the low-energy part of the magnon spectrum is particularly sensitive to the pressure, whereas the higher-energy parts are scarcely affected. This result is a simple consequence of the square-root form of Eq. (47),

which amplifies the changes in $E_{\boldsymbol{k}}$ where the two terms are close to mutual cancellation, i.e., in the vicinity of the band minimum $\boldsymbol{Q}$.

The magnon modes become soft, $E_{\boldsymbol{Q}}=0$, at a critical pressure, p_c, where the enhanced interladder interactions favor a long-ranged AF spin order over a gapped dimer phase. The dimensionless pressure $p(P)$ at the critical pressure for the parameters of $TlCuCl_3$ is

$$p_c=\frac{J-J_1}{J_2+2J_3}\simeq 1.018, \tag{48}$$

from which one notes immediately that the critical pressure represents only a very small fractional increase in p.

Expansion of $\epsilon_{\boldsymbol{k}}$ in Eq. (47) around $\boldsymbol{Q}$, $\epsilon_{\boldsymbol{Q}+\delta\boldsymbol{k}}\simeq\epsilon_{\boldsymbol{Q}}+\delta\epsilon_{\boldsymbol{k}}$, yields a dispersion

$$E_{\boldsymbol{Q}+\delta\boldsymbol{k}}\simeq\sqrt{E_{\boldsymbol{Q}}^2+2J\delta\epsilon_{\boldsymbol{k}}}. \tag{49}$$

Because $\epsilon_{\boldsymbol{k}}$ contains cosine terms in $\boldsymbol{k}$ which are minimal at $\boldsymbol{Q}$, $\delta\epsilon_{\boldsymbol{k}}$ is quadratic in $\delta\boldsymbol{k}$, and at the critical pressure $E_{\boldsymbol{k}}$ has a linear $\boldsymbol{k}$-dependence around $\boldsymbol{Q}$ [Fig. 10]. This stands in explicit contrast to the case of field-induced order, where the single low-lying magnon retains a quadratic dependence on $\boldsymbol{k}$ at the critical field where it softens.

Increasing the pressure beyond p_c induces the AF ordered phase, which may be described by the same operator transformation as in Sec. III. In the absence of an applied magnetic field, the coupled triplets t_+ and t_- are equivalent and $f=g=1/\sqrt{2}$ ($\phi=\pi/4$) in Eq. (23). We note here that this combination in fact restores the eigenvectors t_x and t_y in Eq. (1), referred to above as the ''natural basis'' for the field-free problem. Using the b operators defined in Eq. (23), the Hamiltonian at quadratic order takes the symmetrical form

$$\mathcal{H}_0+\mathcal{H}_{\pm}=\sum_{\alpha=+,0,-}\mathcal{H}_{\alpha} \tag{50}$$

with

$$\mathcal{H}_{\alpha}=\sum_{\boldsymbol{k}}\left[\epsilon_{\boldsymbol{k}\alpha}b_{\boldsymbol{k}\alpha}^{\dagger}b_{\boldsymbol{k}\alpha}+\tfrac{1}{2}(\Delta_{\boldsymbol{k}\alpha}^{\dagger}b_{\boldsymbol{k}\alpha}b_{-\boldsymbol{k}\alpha}+\text{H.c.})\right]. \tag{51}$$

The matrix elements are given by

$$\begin{aligned}
\epsilon_{\boldsymbol{k}+}&=J(u^2-v^2)-8\epsilon_{\boldsymbol{Q}}u^2v^2+(u^2-v^2)^2\epsilon_{\boldsymbol{k}},\\
\epsilon_{\boldsymbol{k}0}=\epsilon_{\boldsymbol{k}-}&=Ju^2-4\epsilon_{\boldsymbol{Q}}u^2v^2+(u^2-v^2)\epsilon_{\boldsymbol{k}},\\
\Delta_{\boldsymbol{k}+}&=(u^2-v^2)^2\epsilon_{\boldsymbol{k}},\\
\Delta_{\boldsymbol{k}0}=-\Delta_{\boldsymbol{k}-}&=\epsilon_{\boldsymbol{k}},
\end{aligned} \tag{52}$$

where

$$u^2=\frac{1}{2}+\frac{J}{(-4\epsilon_{\boldsymbol{Q}})},\quad v^2=\frac{1}{2}-\frac{J}{(-4\epsilon_{\boldsymbol{Q}})} \tag{53}$$

and

$$\epsilon_{\boldsymbol{Q}}=-\frac{1}{2}[J_1+p(J_2+2J_3)]. \tag{54}$$

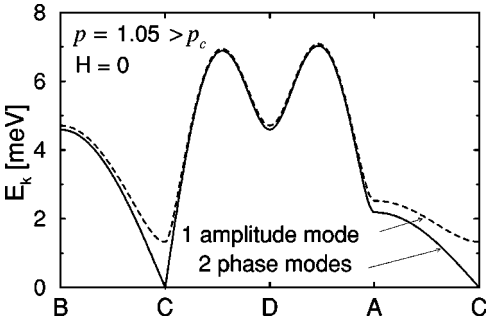

FIG. 11. Magnon dispersion relations in pressure-induced AF phase at zero field, showing two degenerate phase modes (solid line) and one amplitude mode (dashed line).

The magnon mode dispersion relations are then given by

$$E_{\boldsymbol{k}\alpha}=\sqrt{\epsilon_{\boldsymbol{k}\alpha}^2-\Delta_{\boldsymbol{k}\alpha}^2}, \tag{55}$$

and are illustrated in Fig. 11. With this choice of coordinates the staggered magnetic moment is developed along the $\hat{x}$ axis in spin space, as the transformed magnon operator $b_{\boldsymbol{k}+}$ is precisely t_x of Eq. (1). It is clear that the other two modes remain degenerate, and that $E_{\boldsymbol{k}0}$ and $E_{\boldsymbol{k}-}$ are gapless at $\boldsymbol{Q}$ with linear dispersion around this point. These are the spin waves of the ordered magnet, or Goldstone modes; their magnetic moment fluctuates in the plane perpendicular to the induced moment, demonstrating their role as the transverse phase modes. The remaining mode $E_{\boldsymbol{k}+}$ has a finite gap and corresponds to fluctuations in the direction of the induced moment, confirming that this is the longitudinal, or amplitude, mode of the pressure-induced AF phase. This is the splitting of the threefold degenerate triplet modes expected from previous studies of coupling-induced AF order in gapped spin systems.[23,24,28] The excitation gap of the amplitude mode may be written as

$$\begin{aligned}
E_{\boldsymbol{Q}+}&=2uv\sqrt{2+u^2v^2}\\
&=2\sqrt{\left[\frac{1}{4}-\left(\frac{J}{4\epsilon_{\boldsymbol{Q}}}\right)^2\right]\left[2+\frac{1}{4}-\left(\frac{J}{4\epsilon_{\boldsymbol{Q}}}\right)^2\right]},
\end{aligned} \tag{56}$$

and its evolution with applied pressure is shown in Fig. 12.

We turn next to a discussion of the pressure dependence of the interladder superexchange parameters, i.e., to a deter-

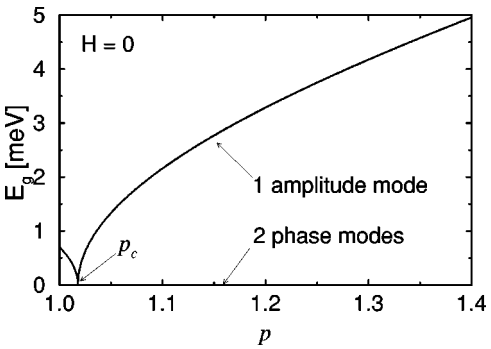

FIG. 12. Pressure-dependence of spin gaps for phase and amplitude modes.

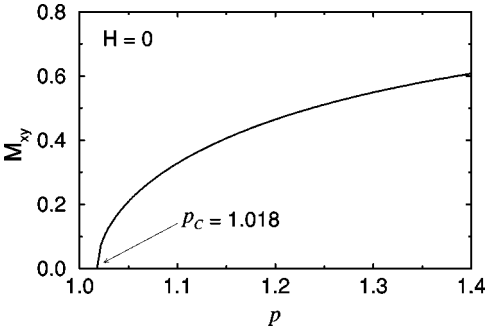

FIG. 13. Pressure-dependence of induced staggered moment M_{xy} in $TlCuCl_3$ at zero field. The normalization is to a saturated moment of 1.

mination of $p(P)$. The staggered moment grows with increasing pressure in the ordered phase as shown in Fig. 13, and close to the critical pressure it has the mean-field exponent $M_{xy} \propto (p-p_c)^{1/2}$. Unlike the field-induced order, there is no uniform magnetization at zero field, which is reflected in the theoretical description by the relation $f=g$. The critical pressure has been found to be approximately $P_c = 2$ kbar.[17] By expanding the function at the critical pressure, a crude determination of $p(P)$ may be made by assuming the form

$$p(P)-p_c=\beta_1(P-P_c)+\beta_2(P-P_c)^2, \tag{57}$$

where β_1 and β_2 are constants to be determined from

$$p_0-p_c=\beta_1(P_0-P_c)+\beta_2(P_0-P_c)^2, \tag{58}$$

$$p_1-p_c=\beta_1(P_1-P_c)+\beta_2(P_1-P_c)^2. \tag{59}$$

The three known data points are (i) atmospheric pressure $P = P_0$, where $p_0=1$; (ii) the critical pressure $P=P_c = 2$ kbar, where $p=p_c=1.018$; and (iii) $P=P_1=1.48$ GPa (14.8 kbar), where the staggered magnetization M_{xy} has attained 60% of its saturation value,[18] which corresponds to $p_1=1.4$ (Fig. 13). With these values the prefactors of the lowest orders in the expansion are $\beta_1=0.012$ kbar^{-1} and $\beta_2=0.0014$ kbar^{-2}. The relative decrease in magnitude of these coefficients suggests that higher orders may not be significant, although a detailed experimental determination is awaited. In the vicinity of the critical pressure, the finite linear term in the pressure dependence of $p(P)$ leads to an exponent $M_{xy} \propto (P-P_c)^{1/2}$. The most important qualitative observation arising from these considerations is that obtaining a critical pressure of $P_c=2$ kbar is straightforward in the laboratory, which in practice implies that experiments probing the properties of the $TlCuCl_3$ system on both sides of the pressure-induced QPT could be performed on samples of considerable volume.

The pressure-dependence of the spin gap of the amplitude mode (56), shown in Fig. 12, is similar to that of the induced staggered moment (Fig. 13), as both depend in a similar manner on the singlet-triplet mixing coefficient θ. Under a pressure of 1.48 GPa, where the neutron-diffraction experiment revealing magnetic order was performed, we estimate the gap of the amplitude mode to be 5 meV. This is well above the value required to distinguish the amplitude mode from the spin waves and magnetic Bragg peaks in INS experiments, which may thus be performed at lower pressures and with larger samples. $TlCuCl_3$ therefore offers an ideal system for observation of the amplitude mode, and for the measurement of its dispersion over a significant portion of the Brillouin zone. These measurements could be used to test the hypothesis that the amplitude mode is broad, and potentially ill-defined, due to the possibility of decay processes into pairs of spin waves.[58] The gap of the amplitude mode may also be measured from the location of additional contributions to susceptibility, nuclear-magnetic-resonance (NMR), and electron-spin-resonance signals.

We conclude this section by noting the two qualitative differences between the pressure-induced QPT and the field-induced situation discussed in Sec. III. The first concerns the breaking of symmetry in real space and in spin space. In the field-induced case the plane of the staggered moment is dictated by the applied magnetic field, and its direction within the plane is determined by a spontaneous breaking of the O(2) symmetry. Rotation of the moment corresponds to the single Goldstone mode. In the pressure-induced case there is no coupling of the spin direction to the crystal axes (in the absence of additional terms in the Hamiltonian which are not introduced here), the development of AF order requires a spontaneous breaking of O(3) symmetry, and two Goldstone modes specify the rotations of the staggered moment. Here we have for convenience chosen the $\hat{x}$ direction, but the results are identical to bond-operator treatments choosing any other symmetry-breaking axis. The second difference concerns the triplet modes participating in the condensate in the bond-operator description. In the field-induced case the applied magnetic field lowers the symmetry of the system in a manner such that only one mode is driven to become massless at the QPT. It is this mode whose mixing into the singlet determines both the primary ground-state properties of the ordered phase and the nature of the phase fluctuation (the Goldstone mode), while the small admixture of the highest triplet is required primarily for consistency. In the pressure-induced case the degeneracy of the magnons is lifted only by the spontaneous breaking of symmetry, and the condensate is composed only of the singlet and the triplet (t_x) which constitutes the amplitude mode, i.e., the Goldstone modes (spin waves) explicitly do not form a part of the condensate. These two features are responsible for the differences between

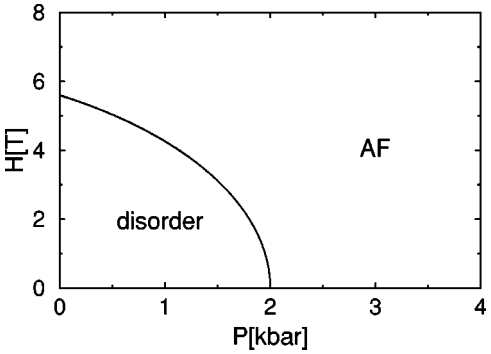

FIG. 14. Phase diagram for the model in the $P-H$ plane.

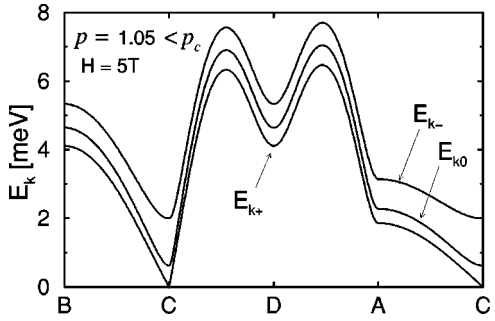

FIG. 15. Magnon dispersion relations in the pressure-induced AF phase under a magnetic field $H=5$ T$<H_c$.

pressure- and field-induced QPTs at the level of quantities such as critical exponents (below). Because the field acts to break the symmetries responsible for the properties of the pressure-induced QPT, any studies of quantum criticality under simultaneous application of finite field and pressure are dominated by the behavior of the field-induced QPT.

B. Finite magnetic field

Magnetic fields and hydrostatic pressure may be regarded as cooperating factors in the stabilization of an AF ordered phase. One may thus determine the phase boundary between magnetically ordered and disordered phases, and this is shown in the estimated $P-H$ phase diagram in Fig. 14. The phase boundary is determined by the condition

$$g\mu_B H=\sqrt{J^2-J[J_1+p(P)(J_2+2J_3)]}. \tag{60}$$

The leading linear dependence of the superexchange on pressure in the vicinity of P_c results in the phase boundary having the form $H_c\propto(P_c-P)^{1/2}$. We note that the phases on both sides of the boundary show considerable evolution across the phase diagram in properties such as the uniform and staggered magnetic moments, and the splitting and dispersion of the magnon modes, as a function of the ratio of H to P.

As noted in the preceding subsection, the degeneracy and dispersion of the magnon modes in the pressure-induced ordered phase are altered significantly in the presence of a magnetic field. A finite field lifts the degeneracy of the transverse spin waves because their spin-fluctuation directions (y and z here) are no longer equivalent. The field causes the mixing of the amplitude mode E_{k+} with the phase mode E_{k-}, and the mixing coefficient changes from $\phi=\pi/4$ at zero field to $\phi=0$ in the high-field limit, where the modes t_+ and t_- are again the appropriate eigenstates. Figure 15 shows the dispersion relations for the three nondegenerate modes at a pressure $p>p_c$ for a finite magnetic field. The qualitative features of the spectra are manifestly dominated by the applied field, and only one Goldstone mode remains. In Fig. 15 we have redefined the lower and upper magnon branches as E_{k+} and E_{k-}, respectively, as in the study of field-induced order (Sec. III).

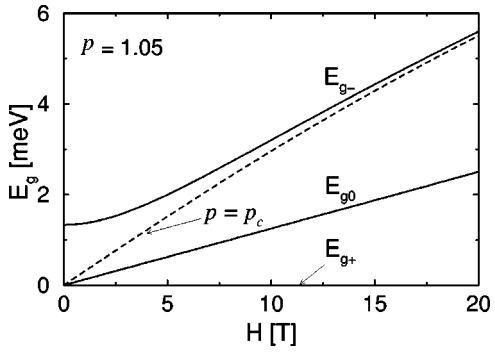

FIG. 16. Magnetic-field dependence of spin gaps in the pressure-induced AF phase, illustrated for $p=1.05$. The dashed line shows the behavior of the highest mode at the critical pressure. The spin gap of the middle branch, which is a spin wave at $h=0$, is the same for $p=p_c$ and $p>p_c$.

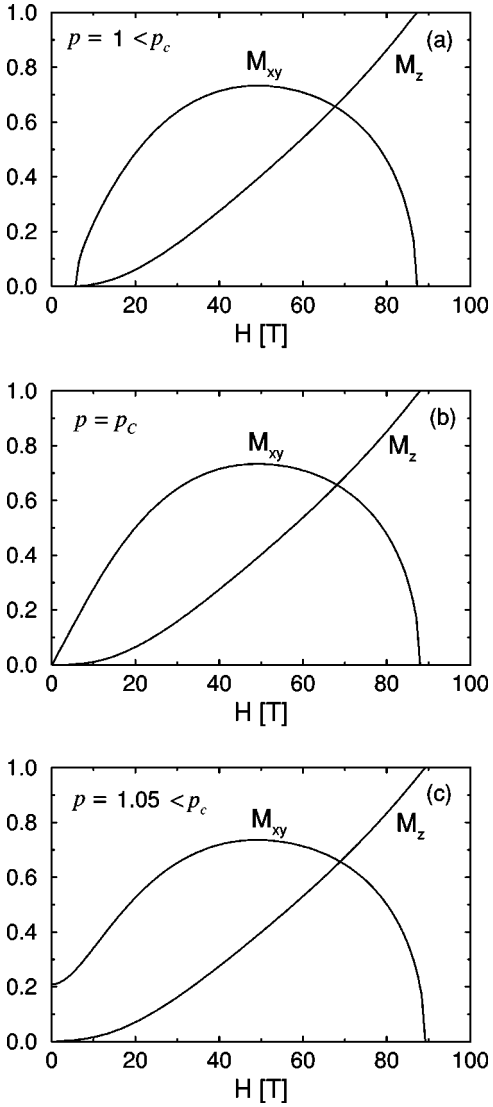

FIG. 17. Normalized magnetization curves for $TlCuCl_3$ (a) in the disordered phase ($p=1<p_c$); (b) at the critical pressure ($p=p_c$); and (c) in the pressure-induced AF-ordered phase ($p=1.05>p_c$). M_z and M_{xy} denote respectively the uniform and staggered magnetizations, and we have taken a g-factor of 2.16.

Figure 16 shows the field dependence of the spin gaps of the three branches in the pressure-induced ordered phase

TABLE II. Exponent for magnetization curves.

	$p<p_c$	$p=p_c$	$p>p_c$
M_z	$\gamma=1$	$\gamma=3$	$\gamma=1$
M_{xy}	$\gamma=\frac{1}{2}$	$\gamma=1$	$\gamma=2$

$p>p_c$, with the same labeling convention as before. The middle branch does not mix with the upper and lower branches even at a finite field, so E_{g0} shows a linear increase from zero which is in fact independent of p for all $p \geqslant p_c$. Because the amplitude mode has a finite excitation gap for $p>p_c$ at $h=0$, the gap grows only quadratically at small fields (linearly at $p=p_c$). It is clear that the amplitude mode is adiabatically connected to the upper magnon branch of the field-only problem ($p<p_c$), which for $p>p_c$ is retrieved in the high-field limit by a continuous alteration of the mixing coefficient ϕ under the external magnetic field.

C. Magnetization

We conclude this section by discussing the uniform and staggered magnetization of $TlCuCl_3$ under finite pressure, for which we define the magnetization exponent near the critical field by

$$\delta M = M(H) - M(H_c) \propto (H - H_c)^{\gamma}. \tag{61}$$

Figure 17 shows the behavior of both magnetization components for the three regimes $p<p_c$, $p=p_c$, and $p>p_c$. In the disordered phase [Fig. 17(a)], the critical field $h_c(p)$ is finite (Fig. 14) and the uniform magnetization M_z shows an apparent nonlinear field dependence over a significant field range, as discussed in Sec. III B. However, close to the critical field the leading power-law dependence is linear ($\gamma=1$), reflecting the fact that the difference between $TlCuCl_3$ and $KCuCl_3$ arising from stronger interdimer coupling is only quantitative in nature. The staggered moment M_{xy} has the mean-field exponent $\gamma=1/2$ expected for a gapped phase (Sec. III B). These exponents may also be deduced by considering the dependence of the magnetizations on the coefficient v^2 [Eqs. (43) and (44)], which specifies the mixing of the triplet magnons into the singlet ground state (23), given that $v^2 \propto H - H_c$ in the disordered phase. Increasing the pressure causes a decrease in $H_c(p)$ until it reaches zero at the critical pressure [$H_c(p_c)=0$] as in Fig. 14. In this case [Fig. 17(b)] both magnetizations develop from $H=0$; the field induces a linear mixing of singlets and triplets in the ground state, $v \propto H$, and M_z depends also on the difference f^2-g^2 of the weights of the t_+ and t_- modes [Eq. (43)], whose field-induced splitting is linear whence $\gamma=3$. M_{xy} is not sensitive to the latter splitting [Eq. (44)], and depends only linearly on the singlet-triplet admixture, yielding $\gamma=1$. Finally, the ordered phase at $p>p_c$ [Fig. 17(c)] has a finite staggered magnetization at zero field, and v has a finite value at $H=0$, leading to $\gamma=1$ for M_{xy}. The uniform component appears to show a similar deviation from linearity as in the disordered phase, but for similar reasons the leading field dependence is in fact linear ($\gamma=1$), close to $H=0$.

The behavior of the two magnetization components in the vicinity of the critical fields is summarized by

$$\delta M_z \simeq \begin{cases} \dfrac{J-2J'}{J'(3J-4J')}(h-h_c) & (p<p_c) \\ \dfrac{1}{(2J')^3}h^3 & (p=p_c) \\ \dfrac{2J'-J}{(2J')^2}h & (p>p_c) \end{cases} \tag{62}$$

for the uniform component, and

$$\delta M_{xy} \simeq \begin{cases} \left[\dfrac{\sqrt{J^2-2JJ'}}{J'(3J-4J')}\right]^{1/2}(h-h_c)^{1/2} & (p<p_c) \\ \dfrac{1}{\sqrt{2}J'}h & (p=p_c) \\ \dfrac{3J-2J'}{8J'^2\sqrt{(2J')^2-J^2}}h^2 & (p>p_c) \end{cases} \tag{63}$$

for the staggered component, where J' denotes the quantity $|\epsilon_{\boldsymbol{Q}}|$ defined in Eq. (54). The magnetization exponents are collected in Table II.

V. SUMMARY

We have used a bond-operator model for $TlCuCl_3$ at zero temperature to provide a complete description of quantum phase transitions (QPTs) in interacting spin–dimer systems driven by both magnetic field and hydrostatic pressure. The magnetically ordered and disordered phases were characterized by analyzing both the dispersion relations of the triplet magnon modes and the staggered and uniform magnetizations as functions of field and pressure. At zero field and ambient pressure, a minimal coupled-dimer model gives a very good account of the magnon dispersions both in $TlCuCl_3$, despite 3D interdimer interactions which are almost sufficiently strong to close the spin gap, and in the structural analog $KCuCl_3$ where interdimer coupling is weaker. At finite fields the bond-operator framework provides a continuous description of the low-field, dimer-singlet phase, the intermediate-field regime of partial (staggered and uniform) magnetic order, and the fully polarized, classical phase at high fields. Under pressure the spin gap of the quantum dimer phase decreases monotonically to a single transition into a phase of staggered magnetic order. The evolution of the order parameters through the QCPs separating these regimes is continuous.

Considering first the gapped system at ambient pressure, the magnetic excitations at low fields are merely the Zeeman-split magnons of the zero-field case, whose dispersion is unaltered by any field up to the lower critical field H_c, where the spin gap is closed. In the high-field regime above H_s, the excitations are precisely the gapped spin waves expected in a fully polarized antiferromagnet. At H_c, a QPT takes place to an intermediate-field phase character-

ized by an antiferromagnetic order of the transverse component of the magnetization, and by one excitation mode which is massless at the Bragg point. This magnon has a ready interpretation as the phase fluctuation mode (Goldstone mode) of a condensate of mixed singlet and triplet character on each dimer rung for fields $H_c<H<H_s$. Because of its gapless nature the phase mode dominates the response of the system at intermediate magnetic fields, including most notably the field-dependence of the magnetization close to the QCPs. The bond-operator description of the ground state is a linear combination of singlets and triplets, which changes continuously from pure singlet character at H_c to a pure triplet state at H_s. The description of the phase mode is in good quantitative agreement with recent INS measurements performed at $H>H_c$.[9]

If the QPT is interpreted as a destabilization of the disordered phase when one or more of its magnon modes become soft, a second route to an ordered phase is provided by the application of hydrostatic pressure to enhance the interdimer interactions and broaden the magnon band. In this situation the gapped magnons of the quantum dimer phase remain triply degenerate as the gap decreases, until at the quantum critical point one obtains a phase with three spin waves. A further increase of the interdimer couplings leads to a conventional antiferromagnet with two spin waves—gapless (Goldstone), transverse, phase modes of the staggered order parameter—accompanied by one longitudinal mode which develops a gap and corresponds to amplitude fluctuations of the staggered moment. The appearance of pressure-induced order in $TlCuCl_3$ has recently been confirmed by experiments[18] which enable one to conclude that the critical pressure for the QPT is very small (a result now confirmed experimentally[17]), thus presenting a valuable additional control parameter for the experimental characterization of QPTs in the $TlCuCl_3$ system.

Both magnetic-field- and pressure-induced ordering transitions can be interpreted as a condensation of low-lying magnon modes, whose linear combination with the singlet describes the ground state of the ordered phase. Indeed, the fact that the modes become soft at wave vector $\boldsymbol{Q}=(0,0,2\pi)$ in both cases suggests a strong similarity between the QPTs driven by both magnetic field and pressure. However, we have shown also that an important, if quantitative, difference exists concerning the degeneracy of the magnon modes and the breaking of rotational symmetry in the ordered phase. While the pressure-induced transition is characterized by two Goldstone modes and a spontaneous breaking of the full O(3) symmetry of spin space, the field-induced transition has only one Goldstone mode corresponding to a spontaneous breaking of O(2) symmetry in the plane normal to the applied field.

Returning to the description of the ordered magnetic phase as a Bose-Einstein condensation (BEC) of magnons, the bond-operator formulation provides considerable additional insight into this approach. The Goldstone mode of the ordered phase corresponds to the linearly dispersive ''sound'' mode connected with BEC. The associated creation and annihilation processes arise from the triplet-triplet interaction $\mathcal{H}_{\rm tt}$, which in the ordered phase generates terms of the form $\bar{a}^2 b_{\boldsymbol{k}+} b_{-\boldsymbol{k}+}$ [Eq. (36)] as a consequence of the condensation of the mode t_+. A recent numerical analysis of the scaling exponents of the magnetization in the ordered regime[59] has confirmed that the BEC scenario provides a suitable description of the QPT, and is universally valid for all interdimer couplings. However, one should be aware that away from the QPT it is necessary to modify the magnon mode that forms the condensate to a linear combination of the dimer singlet and two of the triplet components to describe the ground state in the ordered phase across the entire parameter region.

The theoretical analysis of QPTs is often limited by the absence of suitable descriptions valid simultaneously for the phases on both sides of the transition. Approximate approaches applied in one phase or the other are fated not to converge on a single transition point, and thus cannot provide a continuous evolution in physical properties across the transition. The bond-operator formulation for the magnetic QPTs in spin-dimer systems is appropriate for both disordered and ordered phases, and thus represents an exceptional case illustrating the continuity of physical properties across such transitions. Here we note, however, in the context of $TlCuCl_3$, that two recent, high-resolution experimental studies[60,61] have revealed a small discontinuity at the ordering transition. The weakly first-order magnetic phase transition is accompanied by a simultaneous structural distortion, presumably as a consequence of magnetoelastic coupling which is not included in the present analysis. The nature of this coupled transition awaits further investigation. We comment briefly that the remarkable success of the bond-operator framework for the global phase diagrams of $TlCuCl_3$ and $KCuCl_3$ rests to a considerable extent on the fact that the dimer system has significant coupling in all three spatial dimensions, as a result of which the mean-field approximations employed here are highly accurate. This is reflected in the large value of the singlet condensate parameters in the disordered phases of $TlCuCl_3$ and $KCuCl_3$, which deviate from unity due to quantum fluctuations by at most 3%. The dimensionality of the system is also responsible for the success of the approximation that the constraint is applied only globally. This approach remains appropriate if it is possible for dimer triplets, which are effectively hard-core bosons, to avoid each other by perpendicular hopping processes. Only in one dimension (1D) is this no longer possible, and so the bond-operator treatment of the isolated spin ladder would require a more systematic application of the local constraint in order to reproduce the incommensurate excitations unique to 1D.

We close by summarizing the experimental possibilities offered by the study of QPTs in magnetic systems. While some experiments are now under way to investigate the field-induced QPT, most notably by inelastic neutron scattering to measure the magnon modes both below and above the transition, much scope remains for deeper analysis by techniques including NMR. The application of pressure offers a very promising field for future studies. The experimental result of robust magnetic order at high pressure shows that it is possible to achieve a genuine tuning of superexchange constants through the QPT by the application of hydrostatic pressure. Further, the rather small pressures required imply

the possibility of a variety of measurements, including pressure-dependent specific heat, magnetization, magnetic susceptibility, elastic neutron scattering for the magnetic order parameter and inelastic neutron scattering for magnon dispersion relations. All of these quantities may be measured through the continuous QPT, and in combination with ongoing field-dependent studies yield the possibility of obtaining a complete experimental map of the QPT from magnetic order to quantum disorder in $TlCuCl_3$. We have provided a number of predictions for the properties of the phases in this map, including most notably the evolution of the magnon dispersion relations and the magnetization exponents furnished in Table II. In this connection we also stress the possibility of performing experiments to detect the amplitude mode in the pressure-induced ordered phase, which should be visible in susceptibility and NMR measurements, as well as by inelastic neutron scattering. In conclusion, the phenomena of field- and pressure-induced magnetic order provide excellent examples of quantum phase transitions readily controlled by experiment.

ACKNOWLEDGMENTS

We are indebted to N. Cavadini, H. Kusunose, F. Mila, A. Oosawa, Ch. Rüegg, and H. Tanaka for many valuable discussions. We thank N. Cavadini and Ch. Rüegg for the helpful provision of Fig. 1. This work was supported by the Japan Society for the Promotion of Science (JSPS) and the MaNEP project of the Swiss National Science Foundation.

APPENDIX

Here we present the expressions for $\epsilon_{\boldsymbol{k}i}$ and $\Delta_{\boldsymbol{k}i}$ used in the transformed Hamiltonian (26) at quadratic order in the triplet modes (36). The energies are given by

$$\epsilon_{\boldsymbol{k}+} = (\epsilon_+ f^2 + \epsilon_- g^2)(u^2 - v^2) + C_0 - 2u^2 v^2 \epsilon_{\boldsymbol{Q}} + (u^4 + v^4)\epsilon_{\boldsymbol{k}} - u^2 v^2 [4fg + (f^2 - g^2)^2](\epsilon_{\boldsymbol{k}} + \epsilon_{\boldsymbol{Q}}),$$

$$\epsilon_{\boldsymbol{k}0} = \epsilon_0 - v^2(\epsilon_+ f^2 + \epsilon_- g^2) + C_0 + (u^2 - v^2)\epsilon_{\boldsymbol{k}},$$

$$\epsilon_{\boldsymbol{k}-} = \epsilon_+ g^2 + \epsilon_- f^2 - v^2(\epsilon_+ f^2 + \epsilon_3 g^2) + v^2 (f^2 - g^2)^2 \epsilon_{\boldsymbol{Q}} + C_0 + (u^2 - 4f^2 g^2 v^2)\epsilon_{\boldsymbol{k}},$$

$$\epsilon_{\boldsymbol{k}\pm} = u(-\epsilon_+ + \epsilon_-) fg - uv^2(1 - 2fg)(f^2 - g^2)(\epsilon_{\boldsymbol{k}} + \epsilon_{\boldsymbol{Q}}),$$

$$\epsilon_\alpha = J - \alpha h \qquad (\alpha = +, 0, -), \tag{A1}$$

where $\epsilon_{\boldsymbol{k}}$ is given by Eq. (18) and

$$C_0 = -\epsilon_{\boldsymbol{Q}}[2u^2 v^2(1 + 2fg) - v^4 (f^2 - g^2)^2], \tag{A2}$$

and the coefficients of the pairing terms by

$$\Delta_{\boldsymbol{k}+} = -[2u^2 v^2 - 2fg(u^4 + v^4) + u^2 v^2 (f^2 - g^2)^2]\epsilon_{\boldsymbol{k}},$$

$$\Delta_{\boldsymbol{k}0} = (u^2 + 2fgv^2)\epsilon_{\boldsymbol{k}},$$

$$\Delta_{\boldsymbol{k}-} = -(u^2 + v^2 2fg) 2fg \epsilon_{\boldsymbol{k}},$$

$$\Delta_{\boldsymbol{k}\pm} = (u^3 + 2fguv^2)(f^2 - g^2)\epsilon_{\boldsymbol{k}}. \tag{A3}$$

[1] K. Takatsu, W. Shiramura, and H. Tanaka, J. Phys. Soc. Jpn. **66**, 1611 (1997).
[2] W. Shiramura, K. Takatsu, H. Tanaka, K. Kamishima, M. Takahashi, H. Mitamura, and T. Goto, J. Phys. Soc. Jpn. **66**, 1900 (1997).
[3] A. Oosawa, M. Ishii, and H. Tanaka, J. Phys.: Condens. Matter **11**, 265 (1999).
[4] N. Cavadini, G. Heigold, W. Henggeler, A. Furrer, H.-U. Güdel, K. Krämer, and H. Mutka, Phys. Rev. B **63**, 172414 (2001).
[5] A. Oosawa, T. Kato, H. Tanaka, K. Kakurai, M. Müller, and H.-J. Mikeska, Phys. Rev. B **65**, 094426 (2002).
[6] H. Tanaka, A. Oosawa, T. Kato, H. Uekusa, Y. Ohashi, K. Kakurai, and A. Hoser, J. Phys. Soc. Jpn. **70**, 939 (2001).
[7] N. Cavadini, Ch. Rüegg, A. Furrer, H.-U. Güdel, K. Krämer, H. Mutka, and P. Vorderwisch, Phys. Rev. B **65**, 132415 (2002).
[8] Ch. Rüegg, N. Cavadini, A. Furrer, K. Krämer, H.-U. Güdel, P. Vorderwisch, and H. Mutka, Appl. Phys. A: Mater. Sci. Process. **74**, S840 (2002).
[9] Ch. Rüegg, N. Cavadini, A. Furrer, H.-U. Güdel, K. Krämer, H. Mutka, A. Wildes, K. Habicht, and P. Vorderwisch, Nature (London) **423**, 62 (2003).
[10] A. Oosawa, T. Takamasu, K. Tatani, H. Abe, N. Tsujii, O. Suzuki, H. Tanaka, G. Kido and K. Kindo, Phys. Rev. B **66**, 104405 (2002).
[11] T. Kato, K. Takatsu, H. Tanaka, W. Shiramura, M. Mori, K. Nakajima, and K. Kakurai, J. Phys. Soc. Jpn. **67**, 752 (1998).
[12] N. Cavadini, W. Henggeler, A. Furrer, H.-U. Güdel, K. Krämer, and H. Mutka, Eur. Phys. J. B **7**, 519 (1999).
[13] N. Cavadini, G. Heigold, W. Henggeler, A. Furrer, H.-U. Güdel, K. Krämer, and H. Mutka, J. Phys.: Condens. Matter **12**, 5463 (2000).
[14] T. Saha-Dasgupta and R. Valenti, Europhys. Lett. **60**, 309 (2002).
[15] W. Shiramura, K. Takatsu, B. Kurniawan, H. Tanaka, H. Uekusa, Y. Ohashi, K. Takizawa, H. Mitamura, and T. Goto, J. Phys. Soc. Jpn. **67**, 1548 (1998).
[16] M. Matsumoto, Phys. Rev. B **68**, 180403(R) (2003).
[17] H. Tanaka, K. Goto, M. Fujisawa, T. Ono, and Y. Uwatoko, Physica B **329-333**, 697 (2003).
[18] A. Oosawa, M. Fujisawa, T. Osakabe, K. Kakurai, and H. Tanaka, J. Phys. Soc. Jpn. **72**, 1026 (2003).
[19] Z. Tun, W.J.L. Buyers, R.L. Armstrong, K. Hirakawa, and B. Briat, Phys. Rev. B **42**, 4677 (1990), and references therein; K. Kakurai, M. Steiner, and J.K. Kjems, J. Phys.: Condens. Matter **3**, 715 (1991); Z. Tun, W.J.L. Buyers, A. Harrison, and J.A. Rayne, Phys. Rev. B **43**, 13 331 (1991); M. Kenzelmann, R.A. Cowley, W.J.L. Buyers, Z. Tun, R. Coldea, and M. Enderle, *ibid.* **66**, 024407 (2002).
[20] Z. Hiroi and M. Takano, Nature (London) **377**, 41 (1995).
[21] J.-C. Bouloux and J. Galy, Acta Crystallogr., Sect. B: Struct. Sci. **29**, 1335 (1973); S. Taniguchi, T. Nishikawa, Y. Yasui, Y. Kobayashi, M. Sato, T. Nishioka, M. Kotani, and S. Sano, J. Phys. Soc. Jpn. **64**, 2758 (1995).

[22] M. Troyer, H. Kontani, and K. Ueda, Phys. Rev. Lett. **76**, 3822 (1996); M. Troyer, M.E. Zhitomirsky, and K. Ueda, Phys. Rev. B **55**, 6117 (1997).
[23] I. Affleck, Phys. Rev. Lett. **62**, 474 (1989).
[24] I. Affleck and G.F. Wellman, Phys. Rev. B **46**, 8934 (1992).
[25] M.L. Plumer and A. Caillé, Phys. Rev. B **42**, 8783 (1990); Phys. Rev. Lett. **68**, 1042 (1992).
[26] A.V. Chubukov and D.K. Morr, Phys. Rev. B **52**, 3521 (1995).
[27] H.J. Schulz, Phys. Rev. Lett. **77**, 2790 (1996).
[28] B. Normand and T.M. Rice, Phys. Rev. B **56**, 8760 (1997).
[29] F.H.L. Essler, A.M. Tsvelik, and G. Delfino, Phys. Rev. B **56**, 11 001 (1997).
[30] B. Lake, D.A. Tennant, and S.E. Nagler, Phys. Rev. Lett. **85**, 832 (2000).
[31] K. Amaya, N. Yamashita, M. Matsuura, and T. Haseda, J. Phys. Soc. Jpn. **37**, 1173 (1974); K. Amaya and N. Yamashita, *ibid.* **42**, 24 (1977).
[32] M. Tachiki and Y. Yamada, J. Phys. Soc. Jpn. **28**, 1413 (1970); Suppl. Prog. Theor. Phys. **46**, 291 (1970).
[33] G. Chaboussant, P.A. Crowell, L.P. Lévy, O. Piovesana, A. Madouri, and D. Mailly, Phys. Rev. B **55**, 3046 (1997).
[34] P.R. Hammar, D.H. Reich, C. Broholm, and F. Trouw, Phys. Rev. B **57**, 7846 (1998).
[35] G. Chaboussant, Y. Fagot-Revurat, M.-H. Julien, M.E. Hanson, C. Berthier, M. Horvatic, L.P. Lévy, and O. Piovesana, Phys. Rev. Lett. **80**, 2713 (1998).
[36] G. Chaboussant, M.-H. Julien, Y. Fagot-Revurat, M.E. Hanson, L.P. Lévy, C. Berthier, M. Horvatic, and O. Piovesana, Eur. Phys. J. B **6**, 167 (1998).
[37] M.B. Stone, Y. Chen, J. Rittner, H. Yardimci, D.H. Reich, C. Broholm, D.V. Ferraris, and T. Lectka, Phys. Rev. B **65**, 064423 (2002).
[38] B.C. Watson, V.N. Kotov, M.W. Meisel, D.W. Hall, G.E. Granroth, W.T. Montfrooij, S.E. Nagler, D.A. Jensen, R. Backov, M.A. Petruska, G.E. Fanucci, and D.R. Talham, Phys. Rev. Lett. **86**, 5168 (2001).
[39] C.A. Hayward, D. Poilblanc, and L.P. Lévy, Phys. Rev. B **54**, R12649 (1996).
[40] R. Chitra and T. Giamarchi, Phys. Rev. B **55**, 5816 (1997).
[41] F. Mila, Eur. Phys. J. B **6**, 201 (1998).
[42] A. Furusaki and S. Zhang, Phys. Rev. B **60**, 1175 (1999).
[43] B. Normand, J. Kyriakidis, and D. Loss, Ann. Phys. (Leipzig) **9**, 133 (2000).
[44] X. Wang and Lu Yu, Phys. Rev. Lett. **84**, 5399 (2000).
[45] T. Nikuni and H. Shiba, J. Phys. Soc. Jpn. **64**, 3471 (1995).
[46] T. Giamarchi and A.M. Tsvelik, Phys. Rev. B **59**, 11 398 (1999).
[47] S. Wessel and S. Haas, Eur. Phys. J. B **16**, 393 (2000); Phys. Rev. B **62**, 316 (2000); S. Wessel, M. Olshanii, and S. Haas, Phys. Rev. Lett. **87**, 206407 (2001).
[48] T. Nikuni, M. Oshikawa, A. Oosawa, and H. Tanaka, Phys. Rev. Lett. **84**, 5868 (2000).
[49] S. Sachdev and R.N. Bhatt, Phys. Rev. B **41**, 9323 (1990).
[50] S. Gopalan, T.M. Rice, and M. Sigrist, Phys. Rev. B **49**, 8901 (1994).
[51] B. Normand and T.M. Rice, Phys. Rev. B **54**, 7180 (1996).
[52] B. Normand, Acta Phys. Pol. B **31**, 3005 (2000).
[53] T. Sommer, M. Vojta, and K.W. Becker, Eur. Phys. J. B **23**, 329 (2001).
[54] M. Matsumoto, B. Normand, T.M. Rice, and M. Sigrist, Phys. Rev. Lett. **89**, 077203 (2002).
[55] T. Barnes and J. Riera, Phys. Rev. B **50**, 6817 (1994).
[56] M. Müller and H.-J. Mikeska, J. Phys.: Condens. Matter **12**, 7633 (2000).
[57] See K. Tatani, K. Kindo, A. Oosawa, and H. Tanaka (unpublished) for data for $TlCuCl_3$.
[58] M. Zhitomirsky (private communication).
[59] O. Nohadani, S. Wessel, B. Normand, and S. Haas, cond-mat/0307126 (unpublished).
[60] E.Ya. Sherman, P. Lemmens, B. Busse, A. Oosawa, and H. Tanaka, Phys. Rev. Lett. **91**, 057201 (2003).
[61] O. Vyaselev, M. Takigawa, A. Vasiliev, A. Oosawa, and H. Tanaka, cond-mat/0306519 (unpublished).